UNCLASSIFIED

REPORT DOCUMENTATION PAGE		READ INSTRUCTIONS BEFORE COMPLETING FORM
1. REPORT NUMBER AEDC-TR-74-51	2. GOVT ACCESSION NO.	3. RECIPIENT'S CATALOG NUMBER
4. TITLE (and Subtitle) ANALYTICAL STUDY OF VENTILATED WIND TUNNEL BOUNDARY INTERFERENCE ON V/STOL MODELS INCLUDING WAKE CURVATURE AND DECAY EFFECTS		5. TYPE OF REPORT & PERIOD COVERED Final Report - February to October 1973 6. PERFORMING ORG. REPORT NUMBER
7. AUTHOR(s) E. M. Kraft, ARO, Inc.		8. CONTRACT OR GRANT NUMBER(s)
9. PERFORMING ORGANIZATION NAME AND ADDRESS Arnold Engineering Development Center Arnold Air Force Station Tennessee 37389		10. PROGRAM ELEMENT, PROJECT, TASK AREA & WORK UNIT NUMBERS Program Element 65802F
11. CONTROLLING OFFICE NAME AND ADDRESS Directorate of Technology (DYFS) Arnold Engineering Development Center Arnold Air Force Station, Tennessee 37389		12. REPORT DATE November 1974 13. NUMBER OF PAGES 57
14. MONITORING AGENCY NAME & ADDRESS(if different from Controlling Office)		15. SECURITY CLASS. (of this report) UNCLASSIFIED 15a. DECLASSIFICATION/DOWNGRADING SCHEDULE N/A

16. DISTRIBUTION STATEMENT (of this Report)

Approved for public release; distribution unlimited.

17. DISTRIBUTION STATEMENT (of the abstract entered in Block 20, if different from Report)

18. SUPPLEMENTARY NOTES

Available in DDC

19. KEY WORDS (Continue on reverse side if necessary and identify by block number)

vertical takeoff aircraft
short takeoff aircraft
wind tunnels
slotted walls
porosity
scale models
mathematical models
upwash interference
porous walls

20. ABSTRACT (Continue on reverse side if necessary and identify by block number)

The wind tunnel boundary interference on a V/STOL model is calculated in a rectangular test section with solid vertical walls and ventilated (perforated or slotted) horizontal walls. The interference is found by applying the small perturbation theory of an incompressible fluid to the boundary value problem. The theory uses an image method in addition to Fourier transforms with an equivalent homogeneous boundary condition on the ventilated wall. The mathematical representation of the V/STOL model

DD FORM 1 JAN 73 1473 EDITION OF 1 NOV 65 IS OBSOLETE

UNCLASSIFIED

20 Abstract (Continued)

accounts for the curvature and decay of the wake. The assumption of a constant wake strength produces a paradox in that the maximum value of the interference factors increases as the initial jet velocity decreases. It is indicated that a realistic representation of the wake decay may be as significant as the wake curvature in assessing interference on pitching moment, tail forces, or blockage effects. The most significant aspect of the analysis shows that nonlinear cross-flow effects at the tunnel boundary are important in the V/STOL case, and a quasi-linear approximation to these effects is introduced into the solution providing good agreement with experimental data.

AFSC
Arnold AFS Tenn

PREFACE

The work presented herein was conducted by the Arnold Engineering Development Center (AEDC), Air Force Systems Command (AFSC), at the request of the Ames Research Center (ARC), National Aeronautics and Space Administration (NASA), under Program Element 65802F. The results of the research were obtained by ARO, Inc. (a subsidiary of Sverdrup & Parcel and Associates, Inc.), contract operator of AEDC, AFSC, Arnold Air Force Station, Tennessee. The work was conducted under ARO Project Nos. PF211 and PF411. The research was conducted from February to October, 1973, and the manuscript (ARO Control No. ARO-PWT-TR-74-30) was submitted for publication on April 1, 1974.

CONTENTS

ILLUSTRATIONS

1.0 INTRODUCTION

In V/STOL testing, a partially ventilated test section (slotted or perforated walls) offers substantial reductions in lift and blockage interference (Refs. 1 and 2). However, except for a few cases, only mathematical models typical of conventional aircraft (i.e. sources and sinks or doublets for blockage interference and horizontally trailing horseshoe vortices for upwash interference) have been employed in ventilated wall analysis. Lo (Ref. 3) simulated a V/STOL model in an ideal slotted tunnel by approximating the wake originating from a rotor by means of a skewed cylinder of vortex rings of constant strength lying in planes parallel to the rotor plane. This was an adaptation of the mathematical model suggested by Heyson (Ref. 4) and Wright (Ref. 5) for application in closed and/or open rectangular tunnels.

A recent review (Ref. 6) of the state-of-the-art of low-speed wind tunnels for V/STOL testing has indicated a need for better mathematical simulation of the V/STOL model with a deflected wake in theoretical approaches to the calculation of wind tunnel boundary interference. Labeled as one of the most important current problems was the curved wake simulation of V/STOL models in wall interference investigations. Heyson (Ref. 7) considered the effect of a uniform strength curved wake in test sections with open and/or closed boundaries and has shown that a correct definition of the wake is necessary if corrections to pitching moment and tail forces are to be realistically assessed. Lo (as indicated in Ref. 1) performed calculations in a tunnel with slotted horizontal and solid vertical walls by distributing vortex rings on an empirically determined curve representing the centerline of a jet in crossflow. Binion (Ref. 1) compared Lo's theory with experimental data and indicated the lack of agreement between theory and experiment may be associated with the boundary condition for a slotted wall.

Both Heyson and Lo assumed that the jet strength along the curved wake was constant. Kirkpatrick (Ref. 8) made an effort to include the decay of the jet strength along the jet path by assuming the ring vortex strength to be proportional to the cosine of the wake angle. This decay seemed excessively large when compared with the rate of decay of a real V/STOL wake. In addition, Kirkpatrick's solutions are inaccurate because limited computer capability did not allow the use of a sufficient number of images for the closed wind tunnel.

The purpose of the present analysis is to determine the wind tunnel boundary interference on a V/STOL model in a rectangular tunnel with ventilated horizontal and solid vertical walls. The mathematical representation of the V/STOL model accounts for the curvature and decay of the wake. Solid vertical walls are selected not only for mathematical convenience, but also because Lo and Binion (Ref. 9) have shown that the upwash interference is insensitive to the porosity of the vertical walls.

2.0 GENERAL ANALYSIS

The flow field is considered three-dimensional and is treated as steady, nonviscous, incompressible, and irrotational for the purpose of determining first-order tunnel wall interference corrections. It is also assumed that the velocity perturbation at the wall caused by the body and the perturbations at the body induced by the wall are small compared with the free-stream velocity. The field equation of an inviscid, incompressible fluid in terms of the perturbation velocity potential (Φ) is the well-known Laplace equation:

$$\nabla^2\Phi = \left(\frac{\partial^2}{\partial X^2} + \frac{\partial^2}{\partial Y^2} + \frac{\partial^2}{\partial Z^2}\right)\Phi = 0 \tag{1}$$

2.1 BOUNDARY CONDITIONS

The tunnel geometry to be considered consists of solid vertical walls and ventilated horizontal walls. For the solid vertical walls, the boundary condition of no flow through the wall is

$$\frac{\partial\Phi}{\partial Y} = 0 \text{ at } Y = \pm b \tag{2}$$

For the ventilated horizontal walls, the homogeneous boundary condition derived by Baldwin, et al. (Ref. 10) is used:

$$\frac{\partial\Phi}{\partial X} \pm \frac{1}{R}\frac{\partial\Phi}{\partial Z} \pm K\frac{\partial^2\Phi}{\partial X\partial Z} = 0 \quad \text{at } Z = \pm h \tag{3}$$

where R is a porosity parameter which accounts for the viscous effects in the slots and must be determined experimentally, and K is a geometric slot parameter derived by Chen and Mears (Ref. 11) for a thin wall as

$$K = \frac{(d - a)}{2} \tan\left[\frac{\pi}{2}\left(1 - \frac{a}{d}\right)\right] \tag{4}$$

where d is the periodic spacing of the slots and a is the slot width. The open area ratio a/d is assumed to be small. The derivation of Eq. (4) is based on the assumptions that both the velocity normal to the slot and the perturbation from the mean flow are small compared with the undisturbed tunnel velocity, that the pressure is constant across the open portions, and that the flow angle is zero on the solid portions of the wall. In addition, it is assumed that the plenum pressure equals the undisturbed free-stream pressure and that walls are taken to be straight and parallel with constant width slots.

Equation (3) contains the boundary conditions for other tunnel walls as limiting forms,

Solid wall	$R \to 0$ or $K \to \infty$	$\Phi_Z = 0$
Free-jet	$K \to 0, R \to \infty$	$\Phi_X = 0$
Ideal slotted wall	$R \to \infty$	$\Phi_X \pm (1/R)\Phi_Z = 0$
Perforated wall	$K \to 0$	$\Phi_X \pm (1/R)\Phi_Z = 0$

For convenience in data presentation, a new slot parameter, $P = (1 + K/h)^{-1}$, and a new porosity parameter, $Q = (1 + 1/R)^{-1}$, are introduced so that the interval $0 \leq P, Q \leq 1$ represents the entire range $0 \leq K, 1/R \leq \infty$.

The boundary condition for an ideal slotted wall tunnel can also be written:

$$\Phi + K\Phi_Z = 0 \quad \text{at } Z = \pm h \tag{5}$$

As stated in the derivation of the general equation [Eq. (4)], a basic assumption used is that both the velocity normal to the slot and the perturbations from the mean flow are small compared with the undisturbed tunnel velocity. However, for high-lift V/STOL models, cross-flow velocities in the test section may become appreciable; thus the velocity near the slots can be quite high. Therefore, near the slotted walls, the quadratic terms of the Bernoulli equation may no longer be neglected as

in the derivation of Eq. (5). A derivation of a new boundary condition based on a heuristical approximation to the quadratic terms of the Bernoulli equation for a high-lift V/STOL model in an ideal slotted tunnel is introduced in Appendix A. The fundamental assumption of the derivation is that the higher cross-flow velocities near a slotted wall caused by a lift-augmented model may be approximated by a uniform, constant cross flow related to the increased lift induced by the lift augmentation device. The resulting quasi-linear[1] boundary condition for an ideal slotted wall takes the form at the horizontal walls

$$\frac{\partial \Phi}{\partial X} \pm \frac{1}{R_e} \frac{\partial \Phi}{\partial Z} \pm K_e \frac{\partial^2 \Phi}{\partial X \partial Z} = 0 \quad \text{at } Z = \pm h \tag{6}$$

where the "pseudo porosity parameter" $(1/R_e)$ is defined by

$$\frac{1}{R_e} = \tan \alpha_o \tag{7a}$$

where α_o is the zero lift angle of attack of the lift-augmented V/STOL model. The "effective slot parameter" (K_e) is twice the classic slot parameter defined by Eq. (4). The new quasi-linear boundary condition has exactly the same form as the general ventilated wall boundary condition, Eq. (3). Also, viscous effects in the slots can be incorporated in the quasi-linear boundary condition by redefining the "pseudo porosity parameter" as

$$\frac{1}{R_e} = \frac{1}{R} + \tan \alpha_o \tag{7b}$$

Hence, a boundary condition of the general form of Eq. (3), can also be used for high-lift V/STOL models.

In addition, the upstream and downstream end conditions

$$\Phi = 0 \quad \text{at} \quad X = -\infty$$

$$\frac{\partial \Phi}{\partial X} = 0 \quad \text{at} \quad X = +\infty \tag{8}$$

must be satisfied.

---

[1]The boundary condition is called quasi-linear in the sense that the quadratic cross-flow velocity is approximated in a linear fashion. In the mathematical sense, Eq. (6) is a fully linear equation.

2.2 MATHEMATICAL REPRESENTATION OF A V/STOL MODEL

The augmented lift of the V/STOL model is considered herein to result from a rotor, lifting fan, or lifting jet. The disturbance potential of a rotor, lifting fan, or lifting jet, is represented by an elliptic vortex cylinder sheet following the path of the wake. Among the mathematical V/STOL models chosen in previous investigations, Heyson (Ref. 12) assumed that the wake flows in a straight line intersecting the lower boundary at some point behind the model and then flows along the floor. Wright (Ref. 5) used a similar model except that the wake was assumed to break through the lower boundary and to have no further influence on the flow field. Lo (Ref. 3) argued from physical grounds that Wright's model is the more reasonable of the two models. Furthermore, while Heyson's model can be readily applied to a closed or open jet where an image system can be used to represent the influence of the boundaries, in the present generalized analysis where an image system does not exist for a ventilated wall, severe mathematical complications arise because of the proximity of the jet wake to the lower boundary in the far downstream. Thus, from a physical and mathematical standpoint, the wake-boundary interaction assumption of Wright will be used.

A jet in cross flow which is used herein to represent the model wake has two essential characteristics. First, the path of the curved jet depends primarily on the initial jet to free-stream velocity ratio and the initial jet deflection angle. Second, the strength of the jet decreases rapidly as the jet progresses downstream because of the mixing process between the jet and the free stream and the viscous action within the jet. In the present work, the jet wake is treated in a linear fashion by assuming that the tunnel boundaries have no influence on the jet trajectory. Hence, the jet path is known a priori and can be defined by existing empirical descriptions such as that by Margason (Ref. 13). Unfortunately, the mathematical description of the jet decay has not been described in the literature; hence, the present work will be restricted to an approximate description of the jet decay. For purposes of analytical integration of the interference potential along the curved jet path (see Section 2.4), the jet path is represented by a series of straight line segments approximately equivalent to the curved path, as shown in Fig. 1. Furthermore, the strength of the jet is assumed constant over each straight line segment but may vary from segment to segment.

The model is assumed to be mounted at the center of the test section and parallel to the tunnel centerline since Lo (Ref. 3) has shown the interference factors to be a weak function of the angle of attack. The

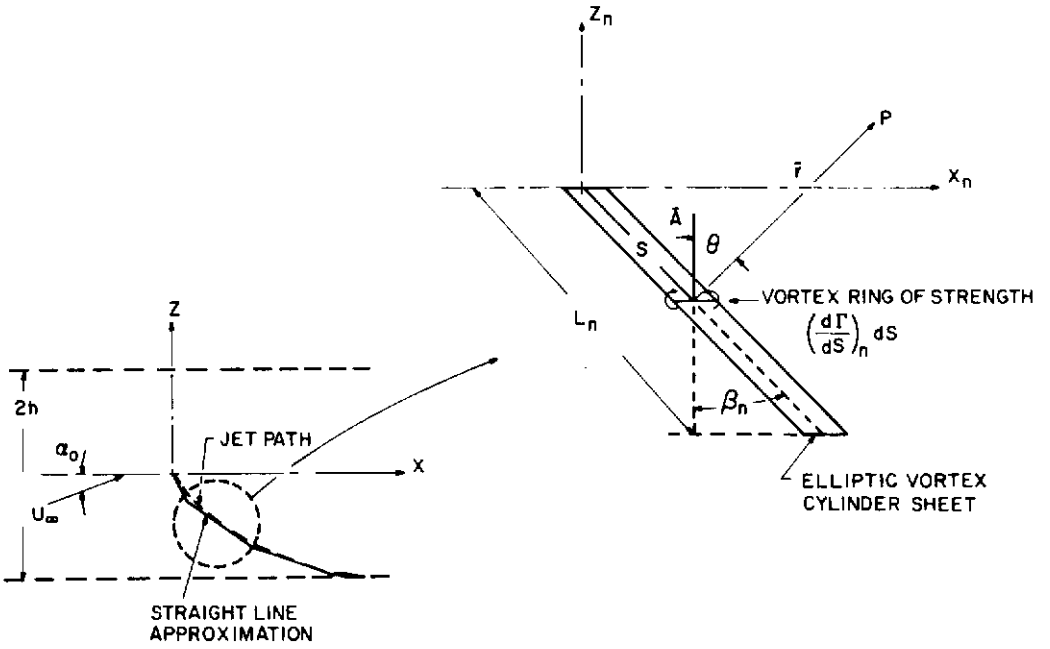

Figure 1. Mathematical representation of V/STOL model.

vortex sheet is made up of a continuous distribution along straight line segments of circular vortex rings lying in planes parallel to the model plane. The element of potential ($d\Phi_m$) induced at a field point P by a vortex ring of strength $(d\Gamma/dS)dS$ is

$$d\Phi_m = (d\Gamma/dS)dS \iint (\cos\theta/4\pi r^2)dA \tag{9}$$

where r is the distance from an element of surface of the vortex ring to the point P, and S is the distance along the jet. By using the small perturbation assumption, the variation of r over the surface A enclosed by the vortex ring is assumed small enough such that the angle θ between the vector $\vec{A}$ and the vector distance $\vec{r}$ is constant. Hence, the integration of Eq. (9) is

$$d\Phi_m = (d\Gamma/dS)dS(A\cos\theta/4\pi r^2) \tag{10}$$

which can be expressed in terms of X, Y, Z, and S for the nth element by using

$$r_n^2 = (X_n - \xi)^2 + Y^2 + (Z_n - \zeta)^2$$

and

$$\cos\theta = \bar{A} \cdot \bar{r}_n / A r_n = (Z_n - \zeta)/r_n$$

where

$$\xi = S \sin\beta_n \quad , \qquad \zeta = -S \cos\beta_n$$

It follows that

$$(d\Phi_m)_n = (A d\Gamma/dS)_n \frac{Z_n - \zeta}{4\pi r_n^3} \, dS \tag{11}$$

Hence the disturbance potential of the nth element is

$$(\Phi_m)_n = \int_o^{L_n} (A d\Gamma/dS)_n \frac{Z_n - \zeta}{4\pi r_n^3} \, dS \tag{12}$$

where the location of the nth element is given by

$$\begin{aligned} X_n &= X - \sum_{j=o}^{n-1} L_j \sin\beta_j \quad , \qquad n = 1, 2, \ldots, N \\ Z_n &= Z + \sum_{j=o}^{n-1} L_j \cos\beta_j \quad , \qquad n = 1, 2, \ldots, N \end{aligned} \tag{13}$$

and L_n is the length of the nth segment. The geometry of the length of the line segments is shown in Fig. 2.

2.3 METHOD OF SOLUTION

By assigning the free-stream velocity (U_∞) and the tunnel half-width (b) as the characteristic velocity and length, the mathematical system can be normalized by defining

$$x = X/b, \quad y = Y/b, \quad z = Z/b, \quad s = S/b, \quad \ell_n = L_n/b$$

$$\phi = \Phi/U_\infty b, \quad \gamma = \Gamma/U_\infty b, \quad F = K/h, \quad \lambda = h/b$$

Thus, the field equation in normalized coordinates is

$$\nabla^2\phi = \left(\frac{\partial^2}{\partial x^2} + \frac{\partial^2}{\partial y^2} + \frac{\partial^2}{\partial z^2}\right)\phi = 0 \tag{14}$$

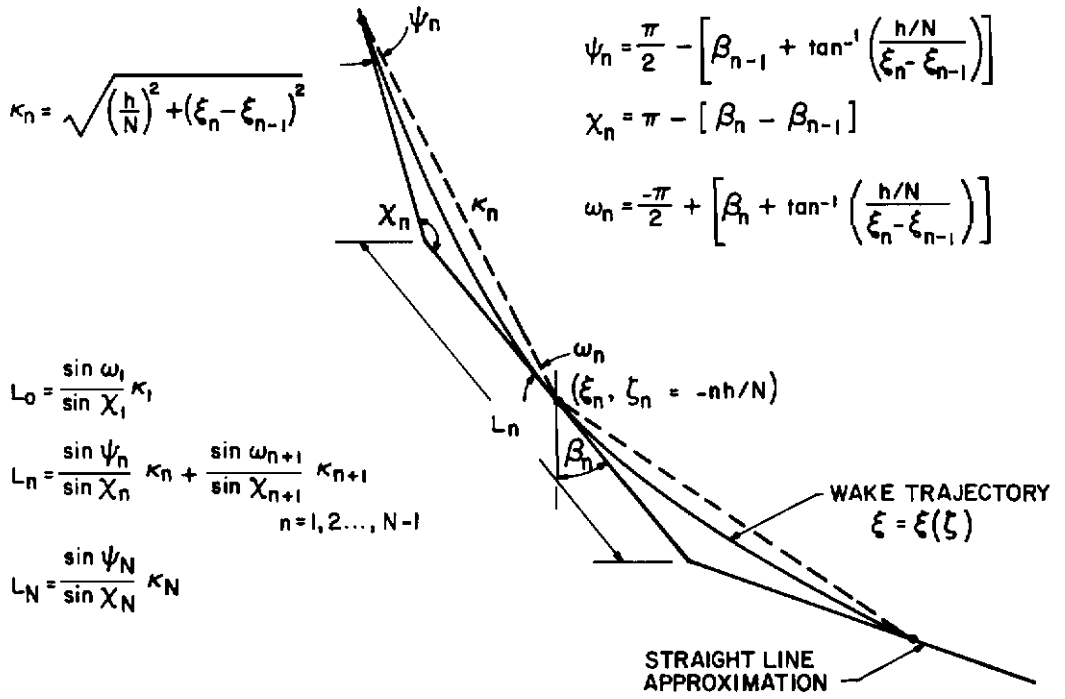

Figure 2. Geometry of straight line approximation to curved jet wake.

with the normalized boundary conditions

$$\frac{\partial \phi}{\partial y} = 0 \quad \text{at } y = \pm 1 \tag{15}$$

$$\frac{\partial \phi}{\partial x} \pm \lambda F \frac{\partial^2 \phi}{\partial x \partial z} \pm \frac{1}{R} \frac{\partial \phi}{\partial z} = 0 \quad \text{at } z = \pm \lambda \tag{16}$$

and

$$\phi = 0 \quad \text{at } x = -\infty \; ; \quad \partial \phi / \partial x = 0 \quad \text{at } x = +\infty \tag{17}$$

The linearity of the field equation and its boundary conditions permits the perturbation potential to be composed of two parts as

$$\phi = \phi_m + \phi_i \tag{18}$$

where ϕ_m is the potential of the flow about the model in free air and ϕ_i is the interference potential induced by the tunnel boundaries.

If ϕ_m is taken to be a known solution of the Laplace equation which approximates the free-air potential at points far from the model, ϕ_i can be calculated from the fact that the sum $(\phi_m + \phi_i)$ satisfies the known boundary condition at the wall. Since the values of ϕ_m are used only at the wall, any approximate representation (ϕ_m) for the model would not appreciably affect the calculation of ϕ_i.

Since the model potential is a series of vortex rings which satisfy Laplace's equation, the differential equation for the interference potential is

$$\nabla^2 \phi_i = 0 \tag{19}$$

The solution of Eq. (19) is obtained by the image method in conjunction with Fourier transforms. An image system consisting of an infinite row of reflected images (shown in Fig. 3) is introduced to satisfy the boundary condition on the solid vertical walls. The expression for the nth element of the curved wake for such an image system, based on Eq. (12), is

$$(\phi_v)_n = \int_0^{\ell_n} (A\,d\gamma/ds)_n \sum_{k=-\infty}^{\infty} \frac{(z_n - \zeta)}{4\pi r_{n_k}^3}\, ds \tag{20}$$

where

$$r_{n_k} = [(x_n - \xi)^2 + (y + 2k)^2 + (z_n - \zeta)^2]^{1/2}$$

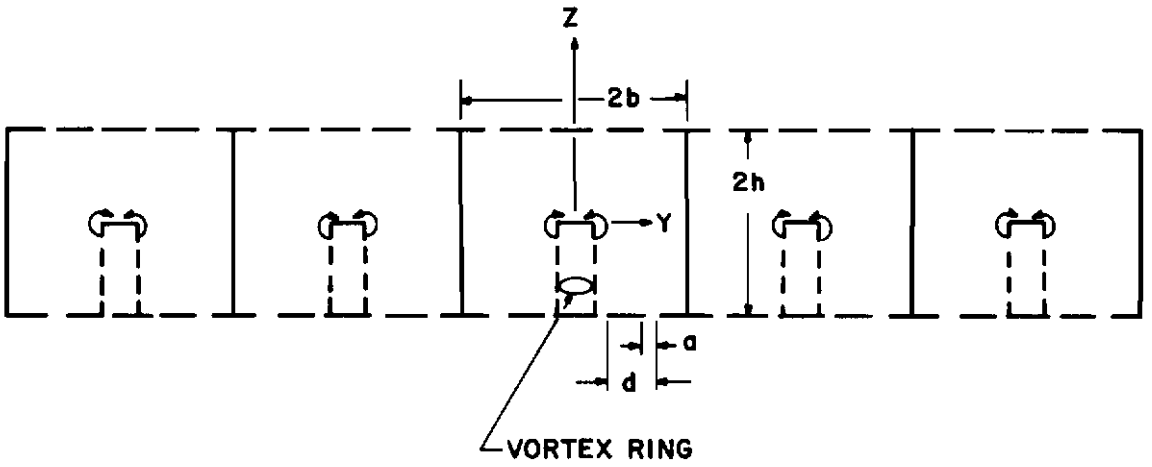

Figure 3. Image system for satisfying boundary conditions on solid vertical walls.

In order to satisfy the boundary condition at the ventilated horizontal walls an additional potential ($(\phi_h)_n$) is required. Consequently, the interference potential for the nth element can be written:

$$(\phi_i)_n = (\phi_h)_n + \left[(\phi_v)_n - (\phi_m)_n\right] \tag{21}$$

Since $(\phi_v)_n - (\phi_m)_n$ is known, it is only necessary to determine $(\phi_h)_n$ to find the interference potential ($(\phi_i)_n$). By substitution, the field equation and boundary conditions for $(\phi_h)_n$ are

$$\nabla^2\phi_h = 0 \tag{22}$$

and

$$\partial\phi_n/\partial y = -\partial\phi_v/\partial y = 0 \quad \text{at } y = \pm 1 \tag{23}$$

$$\partial\phi_h/\partial x \pm (1/R)\partial\phi_h/\partial z \pm \lambda F\partial^2\phi_h/\partial x\partial z = -[\partial\phi_v/\partial x \pm (1/R)\partial\phi_v/\partial z \pm \lambda F\partial^2\phi_v/\partial x\partial z] \quad \text{at } z \pm \lambda \tag{24}$$

$$\phi_h = 0 \quad \text{at } x = -\infty \; ; \; \partial\phi_h/\partial x = 0 \quad \text{at } x = +\infty \tag{25}$$

where the subscript n has been suppressed for convenience.

In order to apply Fourier transforms to Eqs. (22) through (25), the dependent variable should be absolutely integrable (viz, $\phi_h = 0$ at $x = \pm\infty$) over the range $-\infty \le x \le \infty$ (Ref. 14, p. 27). Since it is not, ϕ_h must be replaced by the axial perturbation velocity caused by the horizontal walls (u_h). From the definition,

$$u_h = \frac{\partial\phi_h}{\partial x} \tag{26}$$

and the inverse relation

$$\phi_h = \int_{\bar{x}=-\infty}^{\bar{x}=x} u_h\,dx \tag{27}$$

the field equation yields

$$\nabla^2 u_h = 0 \tag{28}$$

with the boundary conditions

$$\partial u_h/\partial y = 0 \quad \text{at } y = \pm 1 \tag{29}$$

$$u_h \pm \lambda F\partial u_h/\partial z \pm (1/R)\partial/\partial z\left(\int_{\bar{x}=-\infty}^{\bar{x}=x} u_h\,dx\right) = -[\partial\phi_v/\partial x \pm \lambda F\partial^2\phi_v/\partial x\partial z \pm (1/R)\partial\phi_v/\partial z] \quad \text{at } z = \pm\lambda \tag{30}$$

and

$$u_h = 0 \quad \text{at } x = \pm\infty \tag{31}$$

Now it is possible to use Fourier transform techniques.

Applying a complex Fourier transform on x to Eq. (30) yields

$$\bar{u}_h \pm \lambda F \frac{\partial \bar{u}_h}{\partial z} \pm \frac{1}{R} \frac{\partial}{\partial z}\left[\frac{1}{\sqrt{2\pi}} \int_{-\infty}^{\infty}\left(\int_{\underline{X}=-\infty}^{\underline{X}=x} u_h d\underline{x}\right) e^{iqx} dx\right] = -\left[-iq\bar{\phi}_v \pm \left(\frac{1}{R} - iq\lambda F\right)\frac{\partial \phi_v}{\partial z}\right] \tag{32}$$

where the barred functions indicate the transformed variables defined by

$$\bar{g}(q, y, z) \equiv \frac{1}{\sqrt{2\pi}} \int_{-\infty}^{\infty} g(x, y, z) e^{iqx} dx \tag{33}$$

The last term on the left-hand side of Eq. (32) reduces to (Ref. 15, pp. 375 to 376)

$$\pm \frac{1}{R} \frac{1}{(-iq)} \frac{\partial \bar{u}_h}{\partial z}$$

Now applying a finite Fourier cosine transform on y and using Eq. (29), the transformed boundary condition at the ventilated horizontal walls can be written

$$-iq\bar{\bar{u}}_h \pm \left(\frac{1}{R} - iq\lambda F\right)\frac{\partial \bar{\bar{u}}_h}{\partial z} = -(-iq)\left[-iq\bar{\bar{\phi}}_v \pm \left(\frac{1}{R} - iq\lambda F\right)\frac{\partial \bar{\bar{\phi}}_v}{\partial z}\right] \quad \text{at } z = \pm\lambda \tag{34}$$

where

$$\bar{\bar{g}}(q, m, z) = \frac{1}{\sqrt{2\pi}} \int_0^1 \bar{g}(q, y, z) \cos(m\pi y) dy \tag{35}$$

Applying a complex Fourier transform on x to Eq. (20) and using the appropriate convolution theorem yield

$$\bar{\phi}_v(q, y, z) = \frac{1}{\sqrt{2\pi}} \int_0^{\ell} \frac{A d\gamma/ds}{2\pi} (z - \zeta)\left(\sum_{k=-\infty}^{\infty} \frac{K_1(q\rho_k)}{\rho_k}\right) e^{iq\xi} qds \tag{36}$$

where K_1 is the modified Bessel function of order one and

$$\rho_k = \sqrt{(y + 2k)^2 + (z - \zeta)^2} \tag{37}$$

Now applying a finite Fourier cosine transform to Eq. (36) gives

$$\bar{\bar{\phi}}_v(q, m, z) = \int_0^1 \bar{\phi}_v(q, y, z) \cos(m\pi y)dy = \frac{1}{\sqrt{2\pi}} \int_0^{\ell} \frac{A\,dy/ds}{2\pi} q(z-\zeta)H\, e^{iq\xi} ds$$

where

$$H = \sum_{k=-\infty}^{\infty} \int_0^1 \frac{K_1(q\rho_k)}{\rho_k} \cos(m\pi y)dy$$

By following the technique of Acum (Ref. 16), H can be written

$$H = \frac{\pi}{2} \frac{e^{-|z-\zeta|f}}{|z-\zeta|}$$

where

$$f = \sqrt{q^2 + m^2\pi^2}$$

Consequently,

$$\bar{\bar{\phi}}_v(q, m, z) = \frac{1}{\sqrt{2\pi}} \int_0^{\ell} \frac{A\,dy/ds}{4} \frac{(z-\zeta)}{|z-\zeta|} e^{-|z-\zeta|f} e^{iq\xi} ds \tag{38}$$

Transforming the Laplace equation [Eq. (28)] yields the ordinary differential equation:

$$\frac{d^2\bar{\bar{u}}_h}{dz^2} = f^2\bar{\bar{u}}_k \tag{39}$$

which has the general solution:

$$\bar{\bar{u}}_h = A \cosh(fz) + B \sinh(fz) \tag{40}$$

Substituting Eqs. (38) and (40) into Eq. (33) gives

$$\bar{\bar{u}}_h = iq \int_0^{\ell} \frac{A\,dy/ds}{2} \left[(A_1 + iA_2) \sinh(\zeta f) \cosh(zf) + (B_1 + B_2) \cosh(\zeta f) \sinh(zf)\right] e^{iq\xi} ds \tag{41}$$

where A_1, A_2, B_1, and B_2 are given in Appendix B. Applying inverse Fourier transforms on x and y yields

$$u_h(x, y, z) = \frac{1}{\sqrt{2\pi}} \sum_{m=0}^{\infty} j \int_{-\infty}^{\infty} iq \left\{ \int_0^{\ell} \frac{A\,dy/ds}{2} [(A_1 + iA_2) \sinh(\zeta f) \cosh(zf) + (B_1 + iB_2) \cosh(\zeta f) \sinh(zf)] e^{-iq(x-\xi)} ds \right\} \cos(m\pi y)dq \tag{42}$$

where

$$j = \begin{cases} 1, & m = 0 \\ 2, & m \neq 0 \end{cases}$$

Hence from Eq. (27),

$$\phi_h = \frac{-1}{\sqrt{2\pi}} \sum_{m=o}^{\infty} j \int_{-\infty}^{\infty} \left\{ \int_o^{\ell} \left(\frac{A\,d\gamma/ds}{2} \right) \left[(A_1 + iA_2) \sinh(\zeta f) \cosh(zf) + (B_1 + iB_2) \cosh(\zeta f) \sinh(zf) \right] e^{-iq(x-\xi)} ds \right\} \cos(m\pi y) dq$$

$$- \lim_{x \to -\infty} \frac{1}{\sqrt{2\pi}} \sum_{m=o}^{\infty} j \int_{-\infty}^{\infty} \left\{ \int_o^{\ell} \left(\frac{A\,d\gamma/ds}{2} \right) \left[(A_1 + iA_2) \sinh(\zeta f) \cosh(zf) + (B_1 + iB_2) \cosh(\zeta f) \sinh(zf) \right] e^{-iq(x-\xi)} ds \right\} \cos(m\pi y) dq \qquad (43)$$

The last term on the right-hand side can be shown to vanish (Ref. 16, p. 61) as long as the wake is not horizontal. For a horizontal wake, it is obvious that $\xi = s$, $\zeta = 0$, and $\ell \to \infty$, thus the last term of Eq. (43) becomes

$$- \lim_{x \to \infty} \frac{1}{\sqrt{2\pi}} \sum_{m=o}^{\infty} j \int_{-\infty}^{\infty} \left(\frac{A\,d\gamma/ds}{2} \right) (iB_1 - B_2) e^{iqx} \sinh(zf) \cos(m\pi y) \frac{dq}{q} \qquad (44)$$

when the divergent improper integrals are evaluated by the Cesaro method (Ref. 17, p. 361). Finally, Eq. (44) can be written (Ref. 16, p. 61)

$$\lim_{q \to o} \frac{\pi}{\sqrt{2\pi}} \sum_{m=o}^{\infty} jB_1 \sinh(zf) \cos(m\pi y) \left(\frac{A\,d\gamma/ds}{2} \right) \qquad (45)$$

The appearance of Eq. (45) is a consequence of the absolute integrability requirement for the Fourier transform. In a non-horizontal wake, the jet trajectory is assumed to terminate at the lower tunnel boundary at some finite downstream distance, hence the potential induced by the horizontal walls vanishes at infinity thereby satisfying the absolute integrability requirement. However, for a horizontal wake, the vortex cylinder representing the model trails to infinity, hence the potential does not vanish. As discussed in Ref. 18, the omission of the absolute integrability requirement on the Fourier transforms requires the addition of a constant upwash to provide undisturbed flow at $x = -\infty$ for the case of a horizontal wake.

Finally, for a non-horizontal wake, the total interference potential is determined by combining the appropriate terms into Eq. (21) yielding

$$(\phi_i)_n = \frac{-1}{4\pi} \sum_{m=o}^{\infty} j \int_{-\infty}^{\infty} \left\{ \int_o^{\ell_n} \left(\frac{A d\gamma / ds}{2} \right)_n \left[(A_1 + iA_2) \sinh(\zeta f) \cosh(z_n f) + (B_1 + iB_2) \cosh(\zeta f) \sinh(fz) \right] e^{-iq(x-\xi)} ds \right\} \cos(m\pi y) dq \qquad (46)$$

$$+ \int_o^{\ell_n} \left(\frac{A d\gamma / ds}{2} \right) \sum_{\substack{k=-\infty \\ k \neq o}}^{\infty} \frac{(z_n - \zeta)}{2\pi r_{n_k}^3} ds$$

For a horizontal wake, the interference potential is identical to Eq. (53) of Ref. 18. Unfortunately, although a separate solution exists for an exactly horizontal wake, the general solution [Eq. (46)] involves non-uniformly convergent integrals. Hence, in any numerical computation the convergence problem becomes increasingly severe as the wake approaches the horizontal (i.e., $\beta_o \rightarrow \pi/2$ or $U_\infty / U_j \rightarrow \infty$). Therefore, solutions determined from Eq. (46) should exclude nearly horizontal wakes.

Lo (see Ref. 1), in a similar analysis, obtained an equation of the same form as Eq. (46) for a continuously curved jet model in an ideal slotted wall tunnel. He then computed interference factors by numerically integrating the interference potential over the length of the jet. This method proved to be more laborious than the present technique of segmenting the jet trajectory, consequently his numerical computations were restricted to determining the interference at the model location (x = 0). Results of the two techniques are compared in Section 3.0.

2.4 INTERFERENCE FACTORS

The upwash and streamwise components of the interference factor for the model are defined as (Ref. 5):

$$\delta_w = \frac{C}{A} \frac{w_i}{w_o} \qquad (47)$$

and

$$\delta_u = \frac{C}{A} \frac{u_i}{w_o} \qquad (48)$$

where $w_i \equiv \partial\phi_i/\partial z$ is the boundary-induced velocity in the vertical direction, positive downward, and $u_i \equiv \partial\phi_i/\partial x$ is the boundary-induced interference velocity in the stream direction. The upwash interference factor Eq. (47) is, by definition, four times the conventional upwash interference factor for a wing (Ref. 5).

Differentiating Eq. (46) with respect to z and integrating over each of the N straight line segments, the total upwash interference factor is

$$\delta_w = \sum_{n=o}^{N} \frac{(A\,d\gamma/ds)_n}{(A\,d\gamma/ds)_o} \left\{ \frac{-2\lambda}{\pi} \sum_{m=o}^{\infty} j \int_o^{\infty} f \left(\frac{A_1 \sinh(fz_n)}{c_n^2 + d_n^2} \left[R_n \cos(qx_n) - P_n \sin(qx_n) \right] \right.\right.$$

$$+ \frac{A_2 \sinh(fz_n)}{c_n^2 + d_n^2} \left[P_n \cos(qx_n) + R_n \sin(qx_n) \right] - \frac{B_1 \cosh(fz_n)}{c_n^2 + d_n^2} \left[N_n \cos(qx_n) + M_n \sin(qx_n) \right]$$

$$\left.\left. - \frac{B_2 \cosh(fz_n)}{c_n^2 + d_n^2} \left[-M_n \cos(qx_n) + N_n \sin(qx_n) \right] \right) dq \right.$$

$$\left. + \frac{4\lambda}{\pi} \sum_{k=1}^{\infty} (D_n - 3z_n^2 G_n + 6z_n \cos\beta_n F_n - 3\cos^2\beta_n E_n) \right\} \tag{49}$$

where c_n, d_n, D_n, E_n, F_n, G_n, M_n, N_n, P_n, and R_n are defined in Appendix B.

Similarly, the streamwise interference factor is

$$\delta_u = \sum_{n=o}^{N} \frac{(A\,d\gamma/ds)_n}{(A\,d\gamma/ds)_o} \left\{ \frac{2\lambda}{\pi} \sum_{m=o}^{\infty} j \int_o^{\infty} f \left(\frac{A_1 \cosh(fz_n)}{c_n^2 + d_n^2} \left[P_n \cos(qx_n) + R_n \sin(qx_n) \right] \right.\right.$$

$$+ \frac{A_2 \cosh(fz_n)}{c_n^2 + d_n^2} \left[-R_n \cos(qx_n) + P_n \sin(qx_n) \right] + \frac{B_1 \sinh(fz_n)}{c_n^2 + d_n^2} \left[M_n \cos(qx_n) - N_n \sin(qx_n) \right]$$

$$\left.\left. + \frac{B_2 \sinh(fz_n)}{c_n^2 + d_n^2} \left[N_n \cos(qx_n) + M_n \sin(qx_n) \right] \right) dq \right.$$

$$\left. - \frac{12\lambda}{\pi} \sum_{k=1}^{\infty} \left[z_n x_n G_n + \cos\beta_n \sin\beta_n E_n - (z_n \sin\beta_n + x_n \cos\beta_n) F_n \right] \right\} \tag{50}$$

3.0 NUMERICAL RESULTS AND DISCUSSION

3.1 JET TRAJECTORY

The interference factors for the V/STOL model can be computed by numerical integration of Eqs. (49) and (50) once the jet trajectory and jet strength are specified. In the present analysis, Margason's (Ref. 13) empirical jet trajectory is used. In nondimensionalized form, the trajectory is given by

$$x = -\frac{1}{4}\left(\frac{U_\infty/U_j}{d_o/b}\right)^2 z^3 \sec^2 \beta_o - z \tan \beta_o \qquad (51)$$

where U_j is the initial jet velocity, d_o is the initial diameter, and β_o is the initial jet angle. The effect of approximating the jet trajectory by line segments is illustrated in Fig. 4 where the calculated interference factors at the model location (x = 0) in a tunnel with ideal slotted horizontal walls (1/R = 0) are shown for various values of N. The jet strength was assumed to be constant along the jet. It was determined that, for the jet velocity ratios of interest, the curved jet path could be satisfactorily represented by five straight line segments (N = 5).

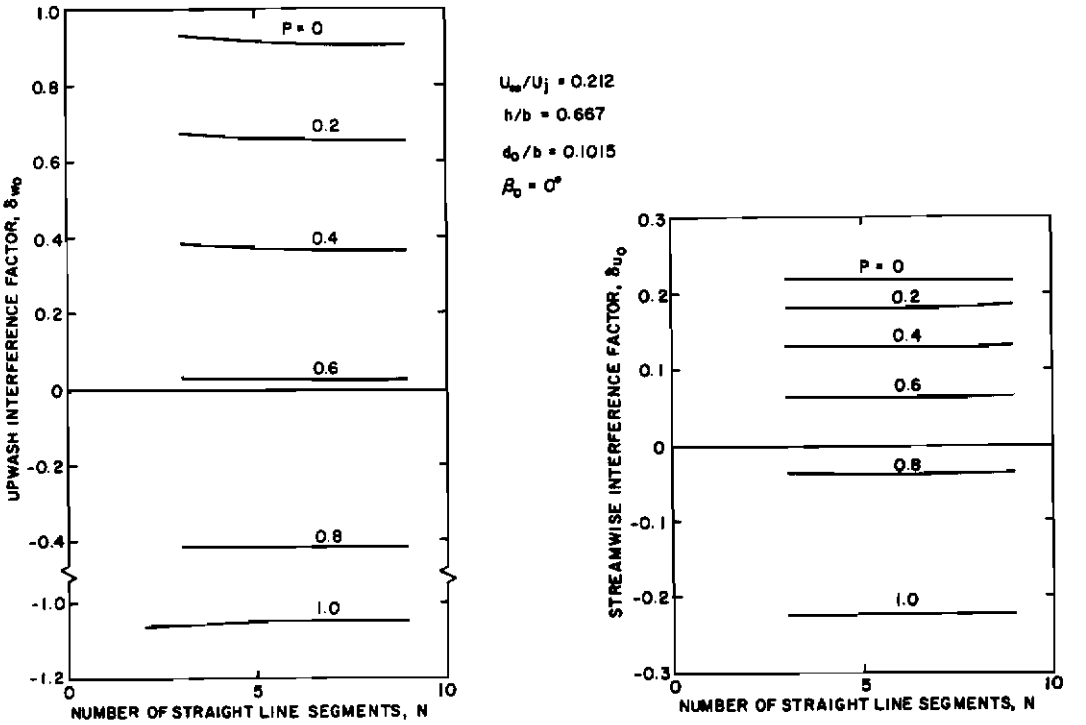

a. Upwash interference factor

b. Streamwise interference factor

Figure 4. Convergence of segmented straight line approximation to curved jet wake.

Typical solutions for the axial distribution of the interference factors in an ideal slotted tunnel[2] for a uniform strength jet are shown in Fig. 5. The x location of the jet intersection point with the tunnel lower boundary is denoted in Fig. 5 by J. I. P. The agreement between the present analysis and the solution of Lo (Refs. 1 or 7) formed by numerical integration along the curved wake is seen to be excellent.

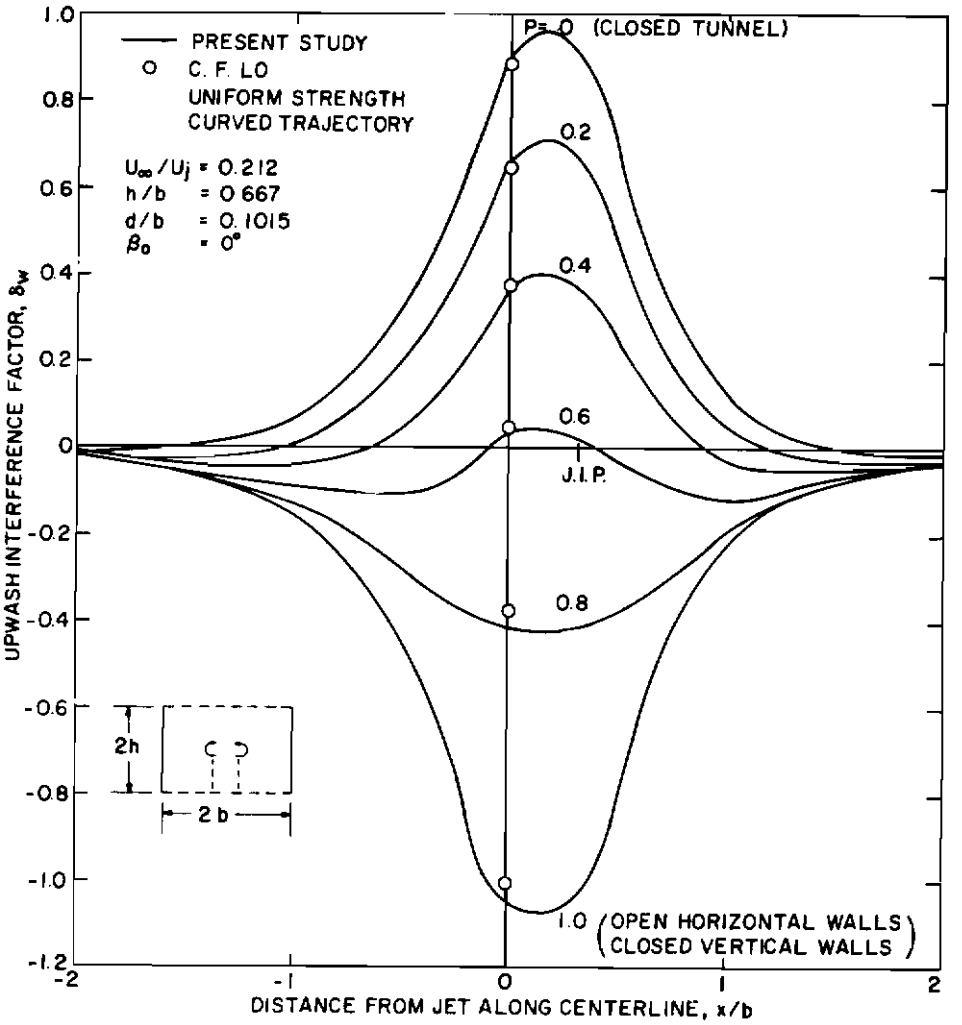

a. Upwash interference factor

Figure 5. Typical axial distribution of interference factors for a constant strength jet in an ideal slotted tunnel.

[2]The terminology slotted (or perforated) wall tunnel refers to the characteristics of the horizontal walls. In all cases, the vertical walls are solid.

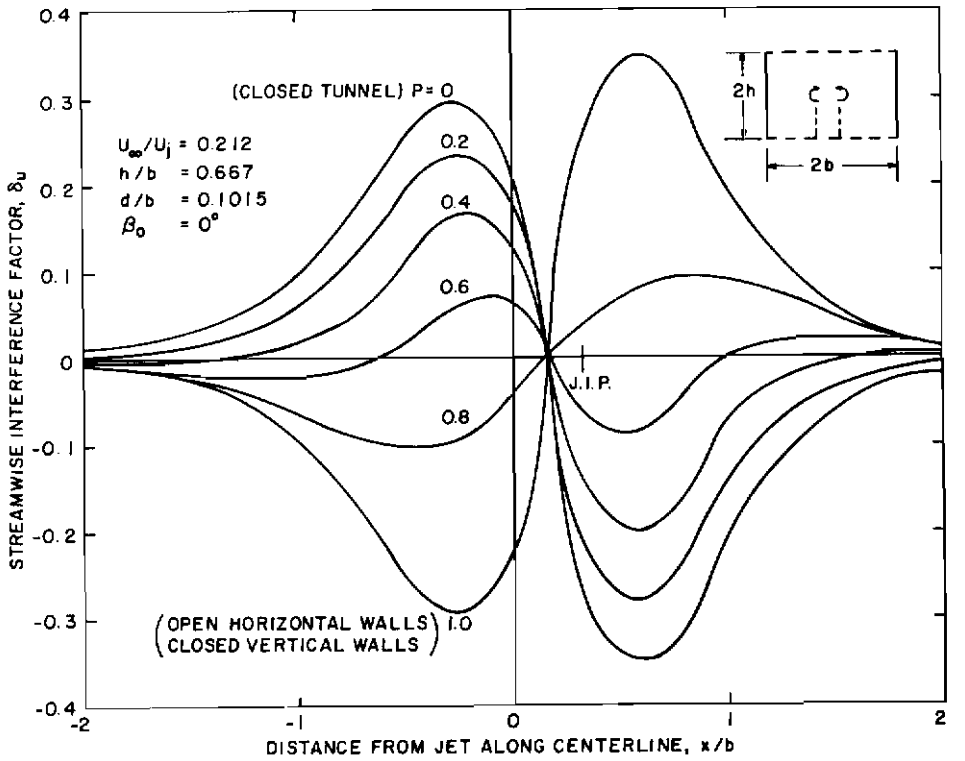

b. Streamwise interference factor

Figure 5. Concluded.

3.2 JET STRENGTH

The calculations shown in Fig. 5 were done assuming a constant strength jet. As long as the initial jet velocity is sufficiently high to cause the jet to intersect the lower tunnel boundary before much decay can occur, the average values of the upwash interference parameter calculated at the model location are not strongly affected by the constant strength jet assumption. However, an obvious paradox arises if a constant strength jet is assumed. For a constant initial jet angle, the interference factors for a weaker jet (corresponding to a longer trajectory before intersecting the lower boundary) are larger in magnitude than for a stronger jet since the constant strength doublets are integrated over a longer length. This paradox is illustrated in Fig. 6 where the axial distributions of the interference factors are compared for two different values of velocity ratio, U_∞/U_j = 0.212 and 0.311. The calculations shown in Fig. 6 were made assuming a constant strength jet and an ideal slotted tunnel. Although the upwash interference factor at the model location (x = 0) seems plausible for the weaker jet (U_∞/U_j = 0.311) when

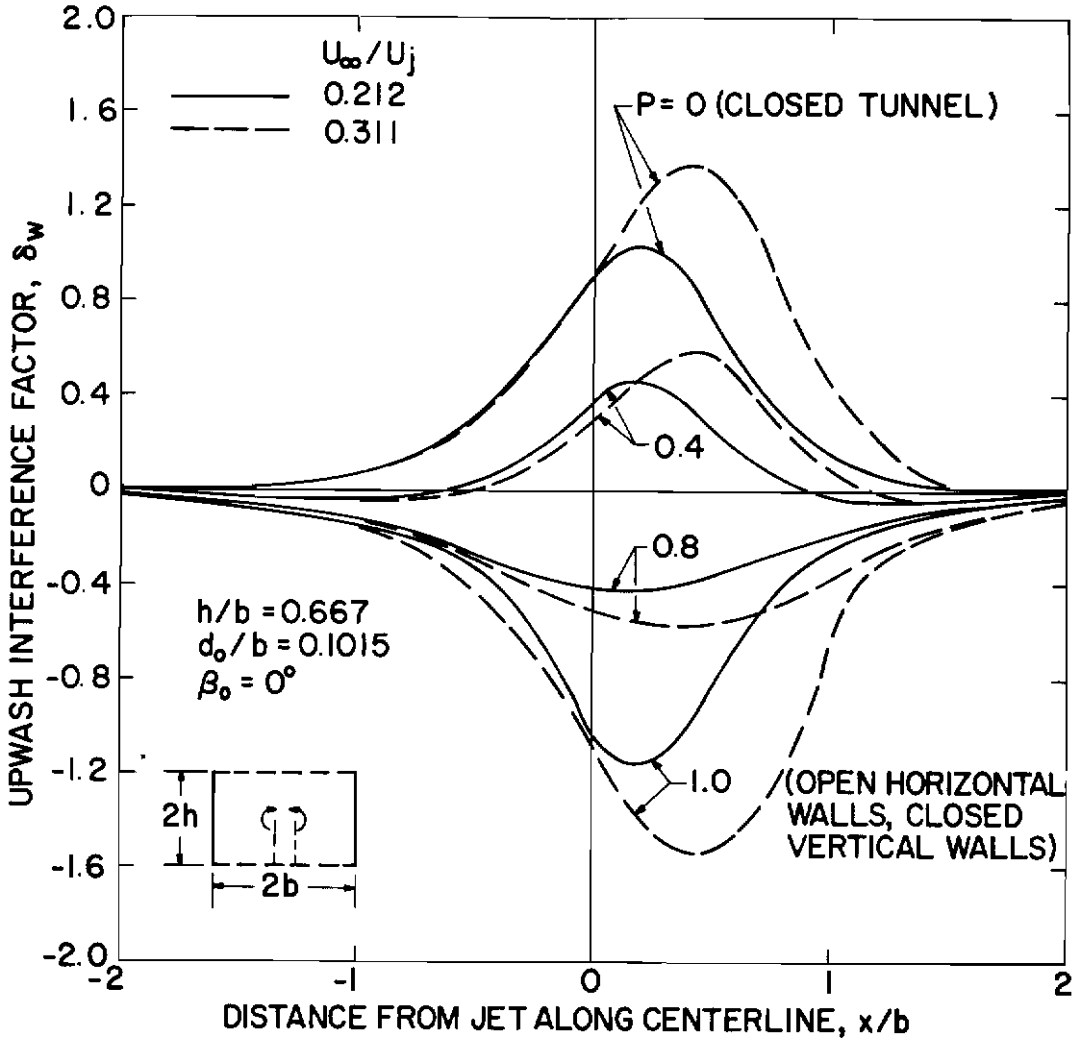

a. Upwash interference factor

Figure 6. Comparison of interference factors for two different constant strength jets in an ideal slotted tunnel.

compared with the stronger jet (U_∞/U_j = 0.212), the interference associated with the weaker jet reaches a much higher maximum magnitude downstream. This is not consistent with any physical interpretation of the real flow field. Furthermore, as shown in Fig. 6b, the streamwise interference factor has a higher magnitude for the weaker jet, even at the model location. Hence, a better description of the jet decay in the tunnel may be as important as the curvature of the jet in the evaluation of pitching moment, tail force, and blockage corrections. Unfortunately, a generalized empirical relation for the jet decay is not available at this time. The idealized mathematical model used in the present analysis is a phenomenological representation for a general V/STOL model with the

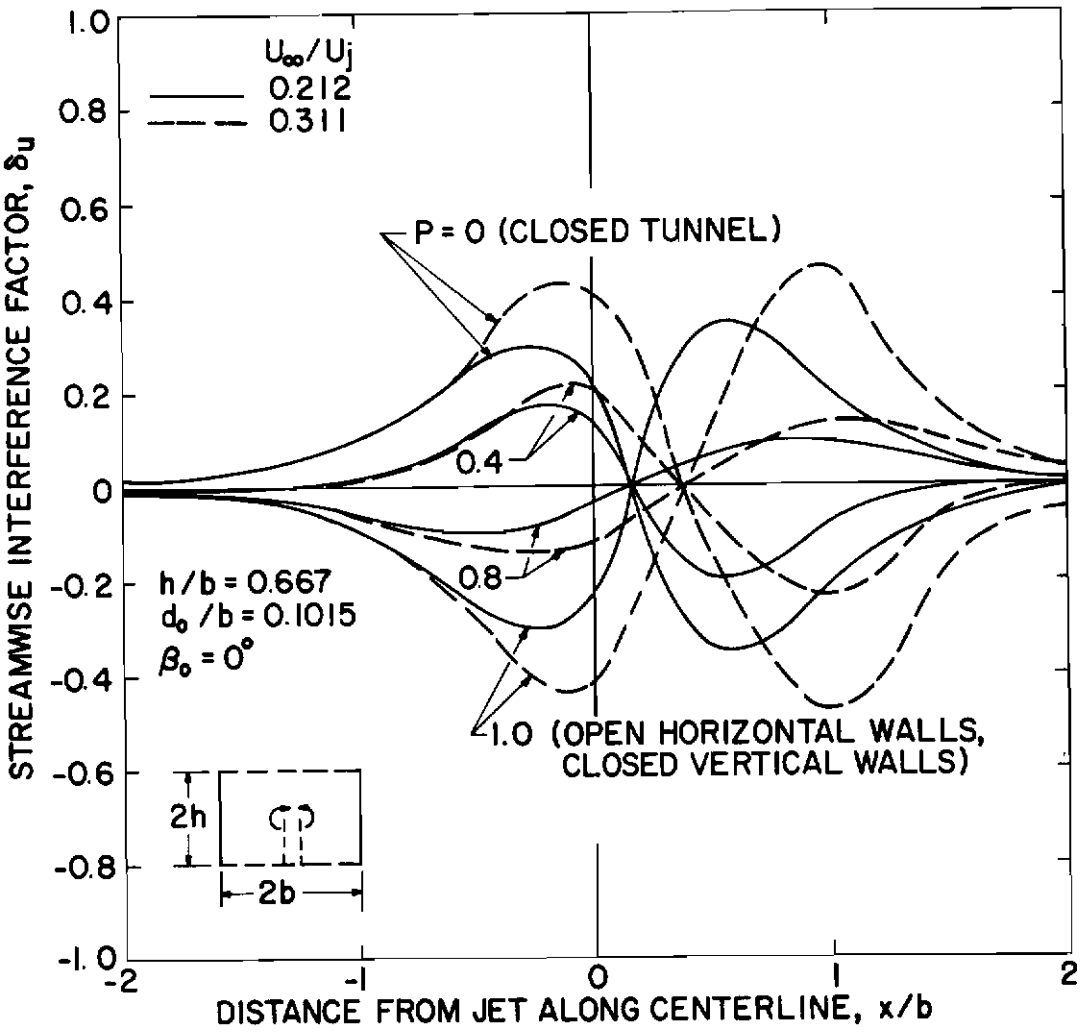

b. Streamwise interference factor

Figure 6. Concluded.

circulation along the jet path being related to the entrainment velocity of a jet in cross flow. Platten and Keffer (Ref. 19) indicate that the entrainment velocity for a jet in cross flow is composed of terms proportional to the velocity excess in the jet (producing entrainment across a turbulent shear layer) and to the shear inflow induced by the vortices developed within the jet. The rate of change of this entrainment velocity is related to the cosine of the trajectory angle. Hence, for an approximation to the decay characteristics of the jet in cross flow represented by the present mathematical model, it may be assumed

$$\left(\frac{d\Gamma}{ds}\right)_n = \left(\frac{d\Gamma}{ds}\right)_o \cos\beta_n \tag{52}$$

which is similar to the decay characteristics assumed by Kirkpatrick (Ref. 8). Actually, Eq. (52) predicts an excessively large decay rate since a vortex motion is known to persist in the far downstream for a jet in cross flow (Ref. 19). However, by comparing the solution for the constant strength jet with the solution for the cosine decay model, an upper and lower limit of the interference factors for a more realistic jet decay model can be formed.

Typical comparisons between a uniform strength and cosine decay wake model in an ideal slotted tunnel are shown in Fig. 7 for the upwash interference factor and in Fig. 8 for the streamwise interference factor.

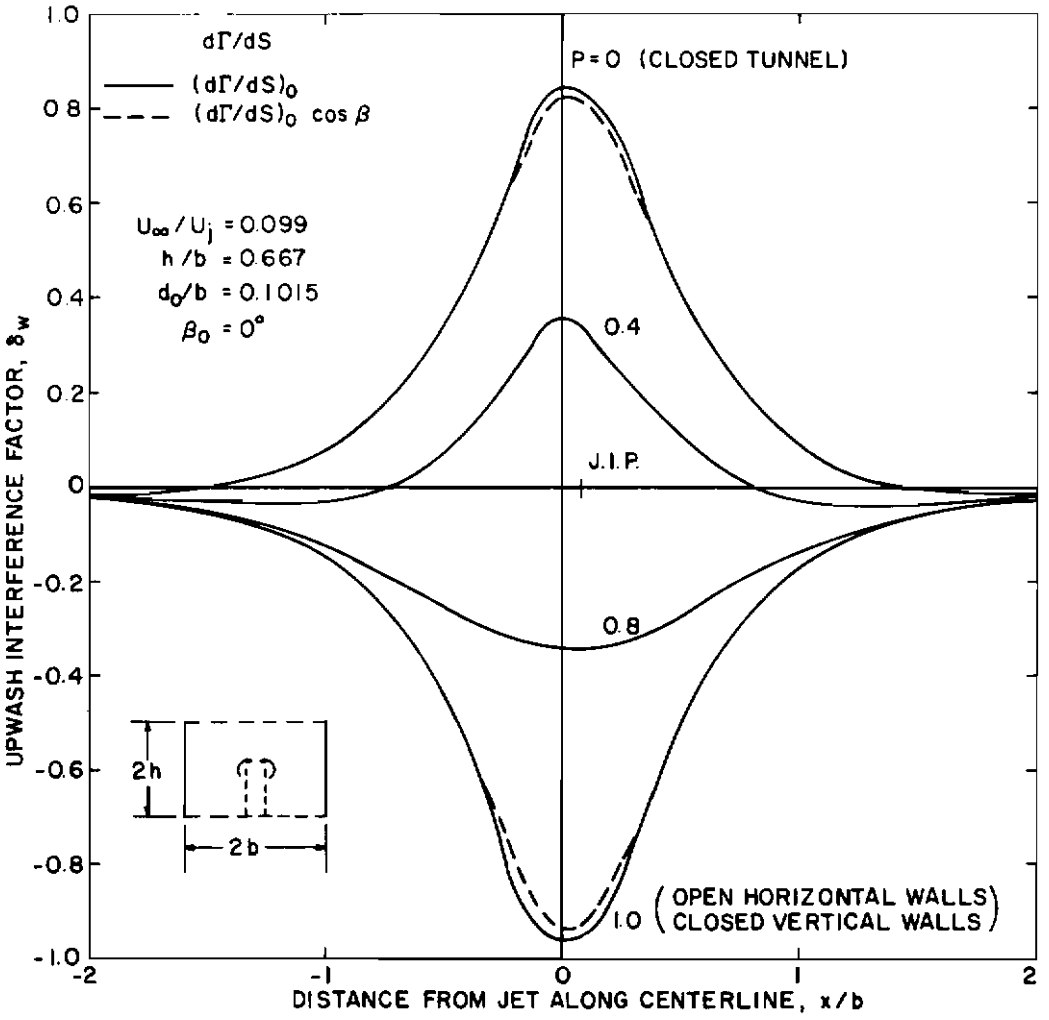

a. $U_\infty/U_j = 0.099$

Figure 7. Comparison of the upwash interference factor in an ideal slotted tunnel for a constant strength and decaying strength jet.

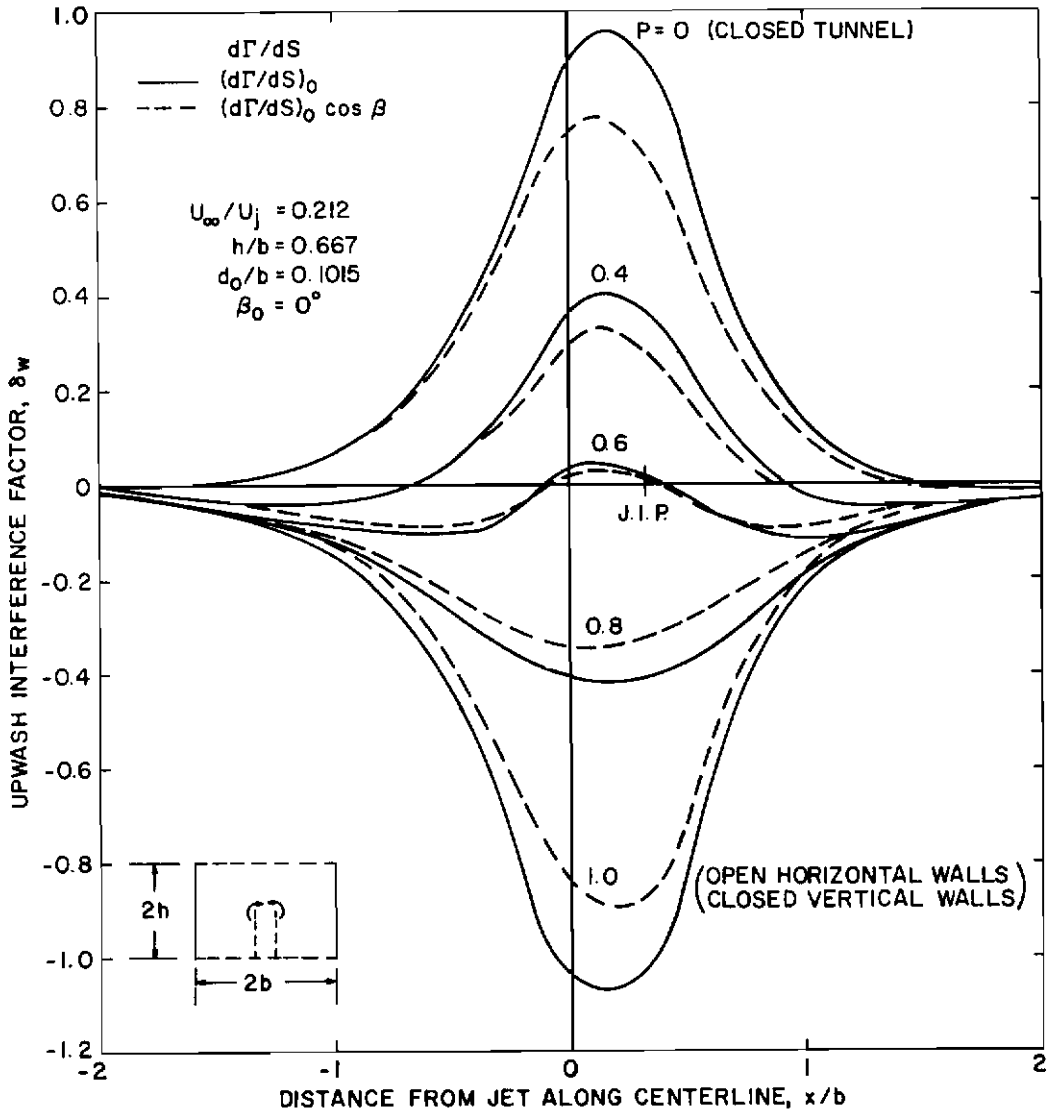

b. $U_\infty/U_j = 0.212$

Figure 7. Continued.

For a high jet velocity as shown in Figs. 7a and 8a, the jet wake intersects the lower tunnel boundary very near the model, hence there is little difference between the constant strength and decaying strength jet models since the latter has not had sufficient length to decay appreciably. However, for a high jet velocity, it should be recognized that the solution may not be applicable since the high energy jet from a real V/STOL lifting system may cause flow reversal when it impinges on the wind tunnel floor (particularly for a closed tunnel). Thus, even though calculations for a high jet velocity minimize the effect of the jet wake simulation, the applicability of such calculations are limited by the criteria for the occurrence of flow breakdown (see Ref. 6 for criteria in closed tunnels).

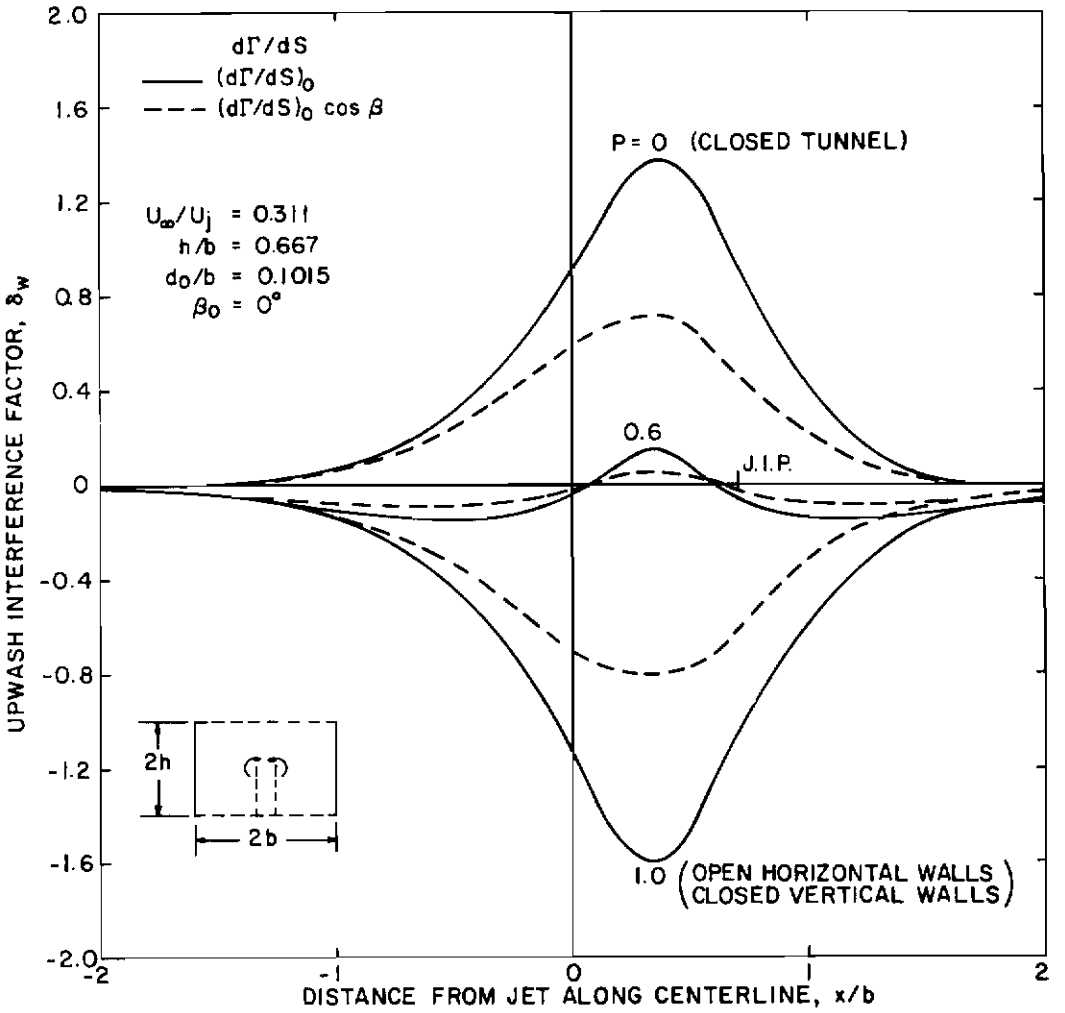

c. $U_\infty/U_j = 0.311$

Figure 7. Concluded.

As the initial jet velocity decreases, the disparity between the constant strength and decaying strength jet increases. Of course, if the jet strength decreases enough, the V/STOL model behaves more like a conventional aircraft, and the details of the jet modeling become irrelevant since the interference factors can be predicted by conventional theories. As the initial jet velocity approaches zero, the paradox which arises by assuming the constant strength jet is emphasized since the maximum value of the interference factors continually increases for the constant strength jet model instead of vanishing.

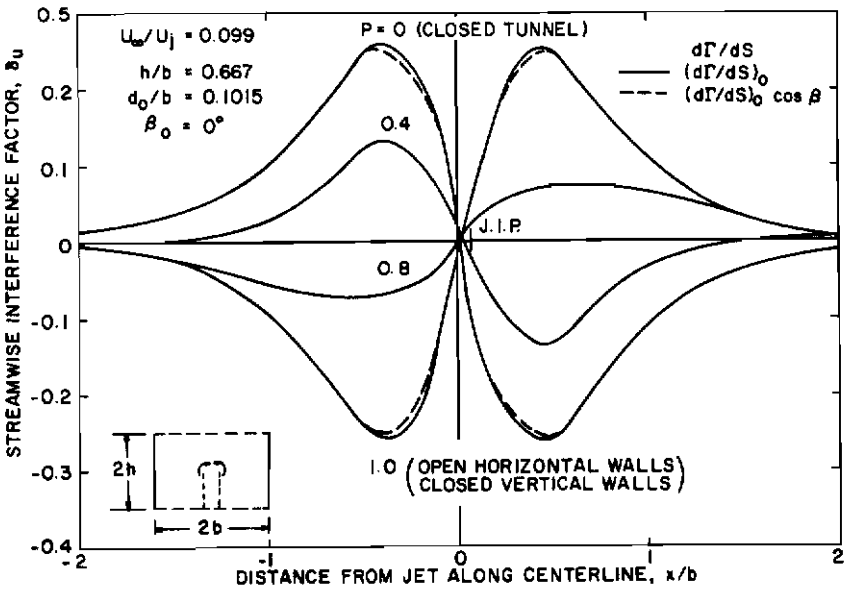

a. U_∞/U_j = 0.099

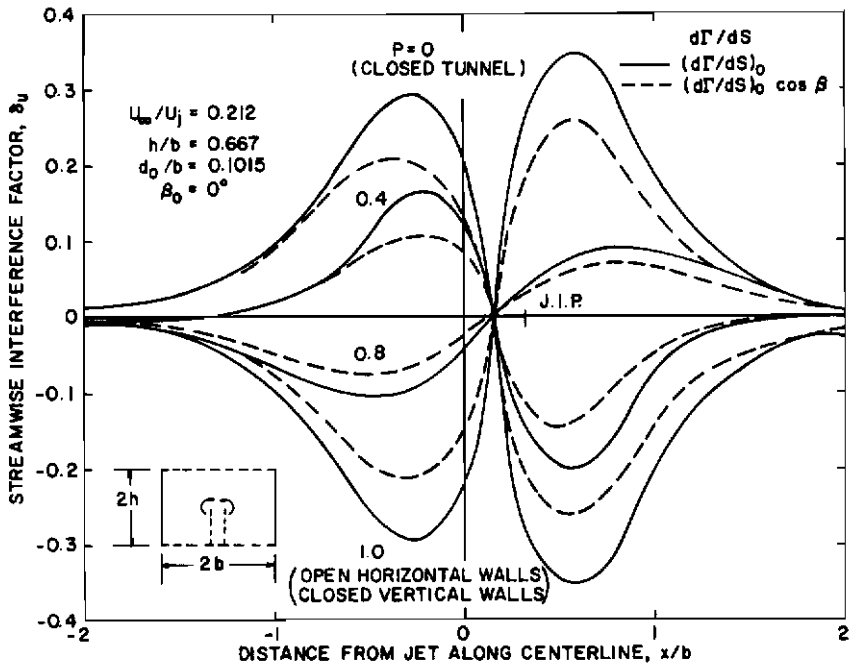

b. U_∞/U_j = 0.212

Figure 8. Comparison of the Streamwise interference factor in an ideal slotted tunnel for a constant strength and decaying strength jet.

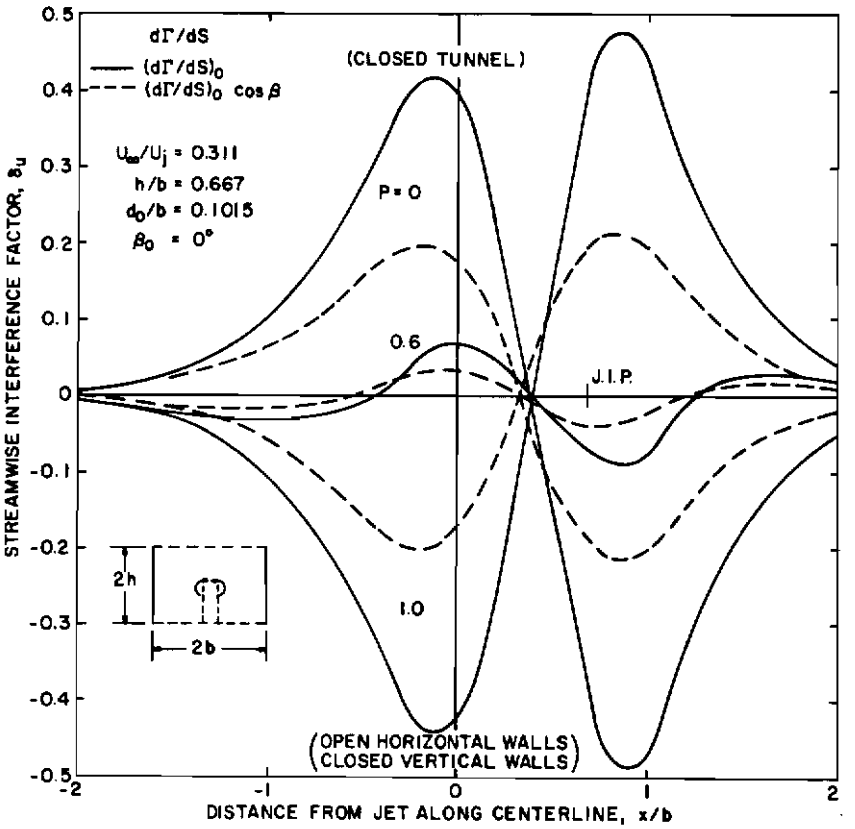

c. $U_\infty/U_j = 0.311$

Figure 8. Concluded.

3.3 OPTIMUM WALL CONFIGURATIONS

For values of the slot parameter (P) at which the interference factors are minimized, the difference between the solutions for the constant strength and decaying strength jets is also minimized (see Figs. 7 and 8). This is an important observation since it indicates that a wall configuration which gives minimum interference may minimize the interference for a wide range of wake representations. The present analysis can, therefore, provide a useful tool for designing minimum interference V/STOL tunnels. A typical application of this utility is shown in Fig. 9 where the slot parameter required to yield zero upwash interference at the model location is shown for various values of jet velocity ratio. The difference in the required slot parameter determined by assuming a uniform strength or decaying strength model is significant. It should be noted, however, that the slot parameter required to minimize the upwash interference may not necessarily be the same as that required to minimize the streamwise interference or streamline curvature effects.

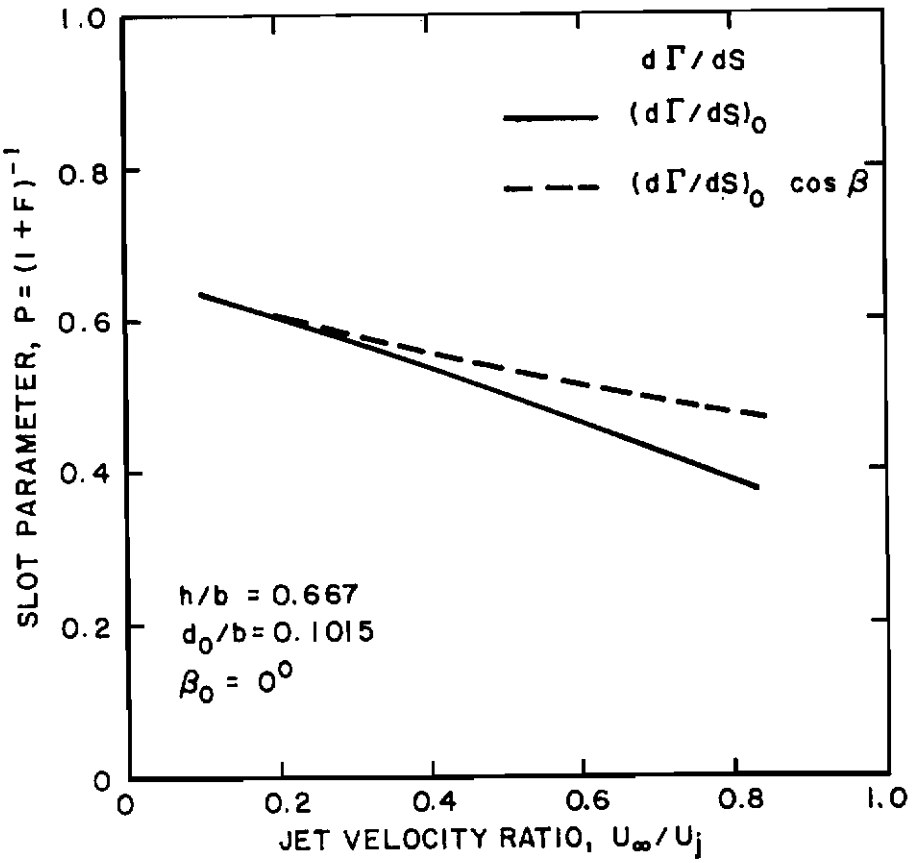

Figure 9. Slot parameter required for zero upwash interference at the model location in an ideal slotted tunnel.

3.4 APPLICATION OF THE QUASI-LINEAR SLOTTED-WALL BOUNDARY CONDITION

The applicability of any theory is predicated on its ability to simulate the actual physical phenomena. Binion (in Ref. 1) compared Lo's theory with the experimentally determined upwash interference on a jet-in-fuselage V/STOL model in a wind tunnel with slotted horizontal walls and solid vertical walls. As indicated in Ref. 1, the lack of agreement between theory and experiment is associated with the slotted-wall boundary conditions rather than the theoretical model. The basic assumptions inherent in the classical ideal slotted-wall boundary condition has been examined in Appendix A, and a quasi-linear homogeneous boundary condition has been formulated to apply to high-lift V/STOL models in wind tunnels with ideal slotted wall. The results of the calculations using the quasi-linear boundary condition are compared in Fig. 10 with

Binion's experimental data and a theoretical calculation using the classic ideal slotted-wall boundary condition. In both calculations, the jet strength was assumed constant since the initial jet velocity ratio was sufficiently high to intersect the lower tunnel boundary before much decay could occur. The agreement between the theory with the quasi-linear boundary condition and the experimental data is seen to be excellent indicating that the nonlinear cross flow effects must be considered in interference calculations in the V/STOL case and the quasi-linear approximation to these effects derived in Appendix A gives a reasonable assessment of the high lift phenomena.

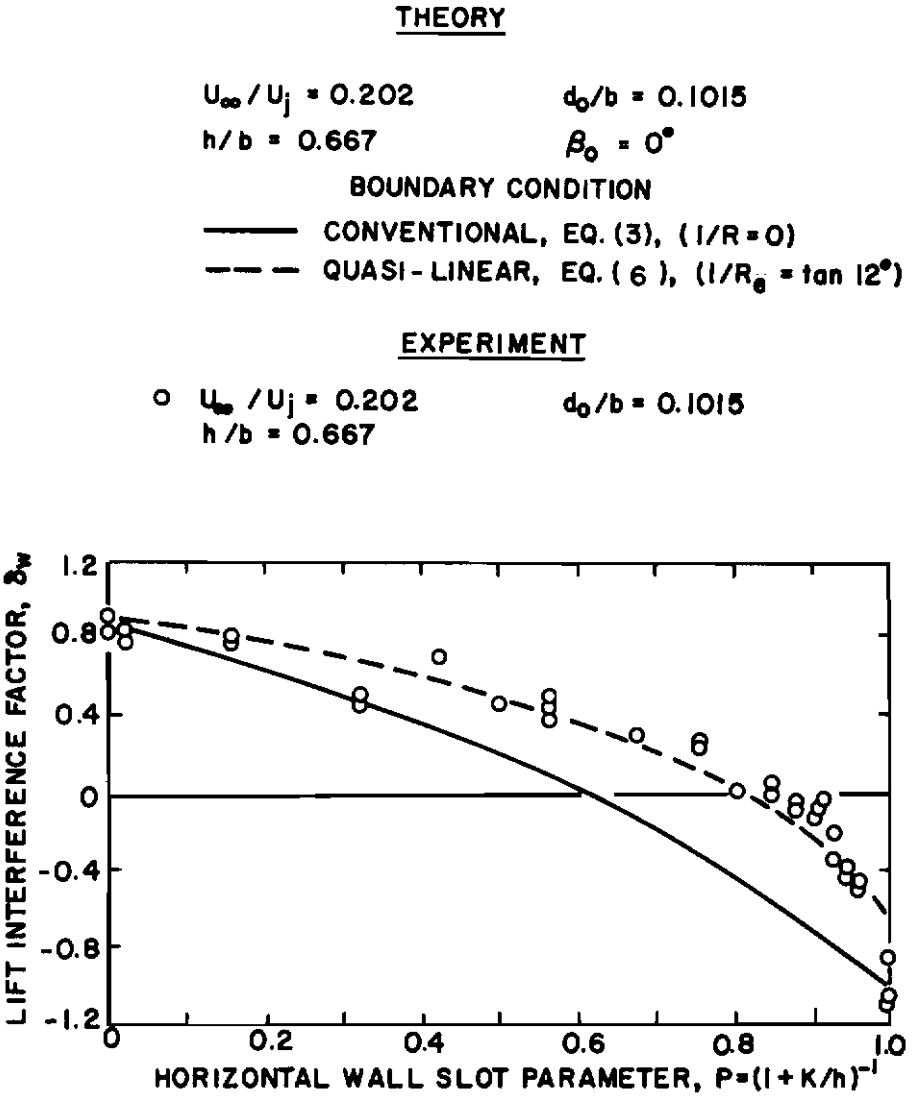

Figure 10. Comparison of theoretical solutions with experiment.

Because of the numerous tunnel and model parameters [h/b, R, K, U_∞/U_j, d_o/b, β_o, $d\Gamma/ds(s)$], it is not feasible to provide a comprehensive set of charts or tables of the interference factors. However, the calculations can be performed quickly for any given set of variables and a listing of the Fortran IV computer program for calculating the interference factors is included in Appendix C to facilitate usage by interested readers.

4.0 CONCLUSIONS

A theoretical investigation of wind tunnel wall interference on V/STOL models in rectangular ventilated wind tunnels has resulted in the following conclusions:

1. The assumption of a constant jet strength produces a paradox in that the maximum value of the interference factors increases as the initial jet velocity decreases.
2. A detailed description of the V/STOL model jet decay may be as important as the curvature of the jet in the evaluation of pitching moment, tail force, and blockage corrections. Furthermore, some approximation to the jet decay is required to overcome the paradox which arises by assuming the constant strength jet.
3. A wall porosity configuration which gives minimum calculated interference may minimize the interference for a wide range of wake representations. Consequently, the details of the theoretical V/STOL model are not essential to determine the porosity criteria for a minimum interference tunnel.
4. The nonlinear cross-flow velocity heretofore not treated in wind tunnel interference calculations is of importance in the analysis of high-lift V/STOL models. A quasi-linear homogeneous boundary condition for ideal slotted walls has been formulated to account for the cross-flow effects in V/STOL testing, and application of the new boundary condition has yielded a significant inprovement in the correlation between theory and experiment.

REFERENCES

1. Binion, T. W., Jr. "An Investigation of Several Slotted Wind Tunnel Wall Configurations with a High Disc Loading V/STOL Model." AEDC-TR-71-77 (AD723294), May 1971.
2. Grunwald, Kalman J. "Experimental Investigation of the Use of Slotted Test Section Walls to Reduce Wake Interference for High-Lift Model Testing." NASA TN-D-6292, June 1971.
3. Lo, C. F. "Wind-Tunnel Boundary Interference on a V/STOL Model." Journal of Aircraft, Vol. 8, No. 3, March 1971, pp. 162-167.
4. Heyson, Harry H. "Jet Boundary Corrections for Lifting Rotors Centered in Rectangular Wind Tunnels." NASA TR-R-71, 1960.
5. Wright, R. H. "Test Section for Small Theoretical Wind-Tunnel Boundary Interference on V/STOL Models." NASA TR-R-286, August 1968.
6. Carbonaro, M. "Review of Some Problems Related to the Design and Operation of Low Speed Wind Tunnels for V/STOL Testing. in "Problems in Wind Tunnel Testing Techniques." AGARD Rpt. 601, April 1973.
7. Heyson, Harry H. "Wind Tunnel Wall Effects at Extreme Force Coefficients." Annual New York Academy of Science, Vol. 154, Article 2, November 1968, pp. 1074-1093.
8. Kirkpatrick, D. L. I. "Wind Tunnel Corrections for V/STOL Model Testing." Master's Thesis, University of Virginia, Charlottesville, Virginia, August 1962.
9. Lo, C. F. and Binion, T. W., Jr. "A V/STOL Wind Tunnel Wall Interference Study." Journal of Aircraft, Vol. 7, No. 1, January-February 1970, pp. 51-57.
10. Baldwin, B. S., et al. "Wall Interference in Wind Tunnels with Slotted and Porous Boundaries at Subsonic Speeds." NASA TN 3176, May 1954.
11. Chen, C. F. and Mears, J. W. "Experimental and Theoretical Study of Mean Boundary Conditions at Perforated and Longitudinally Slotted Wind Tunnel Walls." AEDC-TR-57-20 (AD144314), December 1957.

12. Heyson, H. H. "Linearized Theory of Wind-Tunnel-Jet Boundary Corrections and Ground Effect for VTOL-STOL Aircraft." NASA TR-R-124, 1962.

13. Margason, Richard M. "The Path of a Jet Directed at Large Angles to a Subsonic Free Stream." NASA TN-D-4919, November 1968.

14. Sneddon, I. N. Fourier Transforms. McGraw-Hill Book Company, Inc., New York, 1951.

15. Dettman, J. W. Mathematical Methods in Physics and Engineering. McGraw-Hill Book Company, Inc., New York, 1969. Second Edition.

16. Trantner, C. J. Integral Transforms in Mathematical Physics. John Wiley and Sons, Inc., New York, 1956.

17. Wedder, D. V. Advanced Calculus. Prentice-Hall, Inc., Englewood Cliffs, New Jersey, 1961. Second Edition.

18. Kraft, E. M. "Upwash Interference on a Symmetrical Wing in a Rectangular Ventilated Wall Wind Tunnel: Part I - Development of Theory." AEDC-TR-72-187 (AD757196), March 1973.

19. Platten, J. L. and Keffer, J. F. "Entrainment in Deflected Axisymmetric Jets at Various Angles to the Stream." UTME TP 6808, June 1968.

20. Davis, D. D., Jr. and Moore, Dewey. "Analytical Study of Blockage- and Lift-Interference Corrections for Slotted Tunnels Obtained by the Substitution of an Equivalent Homogeneous Boundary for the Discrete Slots." NACA RM-L53E07b, June 1953.

APPENDIX A
DEVELOPMENT OF QUASI-LINEAR SLOTTED-WALL BOUNDARY CONDITION

An equivalent homogeneous boundary condition for slotted walls [Eq. (5)] has been derived by various authors (e.g., Refs. 10 and 20). In each case, it was assumed that both the slot flow velocities and the perturbations from the mean flow are small compared with the undisturbed tunnel velocity. However, for high-lift V/STOL models, cross-flow velocities in the test section may become appreciable with the velocity near the slots being quite high. Therefore, near the slotted walls, the quadratic terms of the Bernoulli equation may no longer be neglected as in the derivation of Eq. (5). The derivation given below heuristically makes an approximation to the quadratic terms of the Bernoulli equation.

A fundamental assumption is made that the higher cross-flow velocities near a slotted wall induced by a lift-augmented model may be approximated by a uniform, constant cross-flow related to the increased equivalent circulation induced by the lift augmentation device. High-lift V/STOL models characteristically have a large zero-lift angle (α_o) caused by any lift augmentation device. It is assumed that a high-lift model can be represented as a conventional wing at zero angle of attack embedded in a stream with a uniform cross-flow whose velocity is related to the zero lift angle as shown in Fig. A-1.

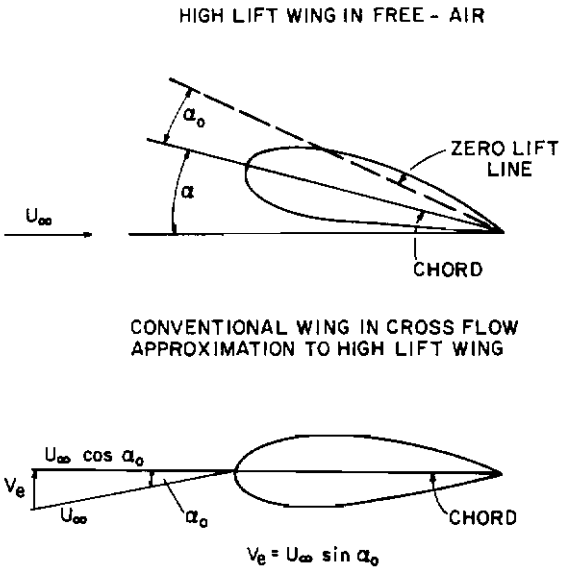

Figure A-1. Representation of a high-lift wing as a conventional wing in uniform cross flow.

When this equivalent system is placed in the wind tunnel, the free-stream static pressure far upstream is given as

$$\begin{aligned} p_\infty &= p_{t_\infty} - \frac{\rho}{2}(U_\infty^2 \cos^2 \alpha_o + V_e^2) \\ &= p_{t_\infty} - \frac{\rho}{2} U_\infty^2 \end{aligned} \tag{A-1}$$

The static pressure at a point inside the test section at the wall is given by

$$\begin{aligned} p &= p_{t_\infty} - \frac{\rho}{2}[(U_\infty \cos \alpha_o + u)^2 + (V_e + w)^2 + v^2] \\ &= p_{t_\infty} - \frac{\rho}{2}[U_\infty^2 + 2uU_\infty \cos \alpha_o + 2wV_e + u^2 + v^2 + w^2] \end{aligned} \tag{A-2}$$

Now, if it is assumed that the pressure just outside the tunnel wall is maintained at p_∞, the pressure difference across the wall is obtained from Eqs. (A-1) and (A-2)

$$\Delta p = p - p_\infty = -\frac{\rho}{2}[2uU_\infty \cos \alpha_o + 2wV_e + u^2 + v^2 + w^2] \tag{A-3}$$

Further, if it is assumed that u, v, w are much smaller than U_∞, then

$$\Delta p \approx -\rho(uU_\infty \cos \alpha_o + wV_e) \tag{A-4}$$

Obviously, for a conventional lifting model, Eq. (A-4) reduces to the well known result for small disturbance theory.

In order to determine the required boundary condition at a slotted wall, it is necessary to find an expression which relates the pressure difference across the wall to the flow through the wall. Consider a thin slotted wall in a field of flow with a uniform velocity normal to the wall in a transverse plane at $-Z_O$ (see Fig. A-2). Because the flow pattern is the same for each slot it is permissible to study a single channel such as the one in which approximate streamlines have been sketched in Fig. A-2. The analysis of the flow near the slotted wall presented here follows closely the development of Davis and Moore (Ref. 20). The kinetic energy enclosed in a region of the flow bounded by the transverse plane at $-Z_O$, by the "walls" of the channel, and by the slot is

$$\text{Kinetic Energy} = \tfrac{1}{2}\rho \iint_A \Phi \frac{\partial \Phi}{\partial n} \, dA \tag{A-5}$$

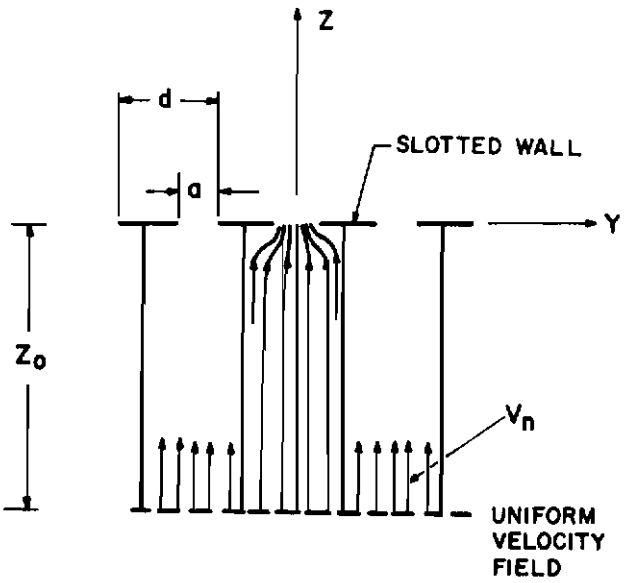

Figure A-2. Schematic of flow field perpendicular to slotted wall.

where the area of integration (A) consists of a surface of unit depth normal to the plane of the page encircling the region shown in Fig. A-2. Since $\partial\Phi/\partial n = 0$ at the channel walls and $\Phi = 0$ at the slot, these regions contribute nothing to the integral. Furthermore, if the transverse plane at $-Z_o$ is sufficiently far away from the slot, the potential $\Phi(-Z_o)$ is essentially constant in this plane, thus

$$\text{Kinetic Energy} = \tfrac{1}{2}\rho\,\Phi(-Z_o)V_nA \tag{A-6}$$

where

$$V_nA = \iint_A \left(\frac{\partial\Phi}{\partial n}\right)_{-Z_o} dA$$

is the volume flow rate. The potential at $-Z_o$ in the presence of a slotted wall has been derived by Chen and Mears (Ref. 11) by replacing the slotted wall by an infinite series of doublets. The result is

$$\Phi(-Z_o) = V_n(-Z_o + K) \tag{A-7}$$

where K is the geometric slot parameter given in Eq. (A-4). Therefore, Eq. (A-6) can be written as

$$\text{Kinetic Energy} = \tfrac{1}{2}\rho(-Z_o + K)V_n^2A \tag{A-8}$$

The portion of the total kinetic energy regarded as being caused by the presence of the slotted wall is $\rho K V_n^2/2$ per unit area.

Now if the slotted wall is replaced by an equivalent homogeneous wall, in the same manner as originally proposed by Busemann (Ref. 20), the energy per unit area at the wall is $\rho K V_n^2/2$. The pressure difference across the slotted wall, which acts in a direction normal to the wall surface must, in potential flow, be equal to the rate of change of momentum associated with the presence of the slots, or

$$\Delta p = \frac{D}{Dt}(\rho K V_n) = \rho K \frac{DV_n}{Dt} \tag{A-9}$$

If it is recognized that $V_n = V_e + w$, the derivative is given as

$$\frac{DV_n}{Dt} = \frac{Dw}{Dt} = \frac{\partial w}{\partial t} + (U_\infty \cos \alpha_o + u)\frac{\partial w}{\partial X} + (Ve + w)\frac{\partial w}{\partial Z} + v\frac{\partial w}{\partial Y} \tag{A-10}$$

For steady flow, and to the same order of approximation used in deriving Eq. (A-4), the pressure difference across the wall is related to the velocity through the wall by

$$\Delta p = \rho K\left(U_\infty \cos \alpha_o \frac{\partial w}{\partial X} + Ve \frac{\partial w}{\partial Z}\right) \tag{A-11}$$

Equating Eqs. (A-11) and (A-4) yields

$$u + \frac{Ve}{U_\infty \cos \alpha_o} w + K\frac{\partial w}{\partial X} + \frac{KVe}{U_\infty \cos \alpha_o}\frac{\partial w}{\partial Z} = 0 \tag{A-12}$$

or in terms of the perturbation potential:

$$\frac{\partial \Phi}{\partial X} + \frac{Ve}{U_\infty \cos \alpha_o}\frac{\partial \Phi}{\partial Z} + K\frac{\partial^2 \Phi}{\partial X \partial Z} + \frac{KVe}{U_\infty \cos \alpha_o}\frac{\partial^2 \Phi}{\partial Z^2} = 0 \tag{A-13}$$

Equation (A-13) is a linear homogeneous boundary condition for the slotted wall in the presence of a uniform cross flow with velocity Ve. By applying the chain rule along a streamline, it is seen that

$$\frac{\partial^2 \Phi}{\partial Z^2} = \frac{\partial w}{\partial Z} = \frac{\partial w}{\partial X}\frac{\partial X}{\partial Z}$$

However, by irrotationality, $\partial w/\partial X = \partial u/\partial Z$. Thus,

$$\frac{\partial^2 \Phi}{\partial Z^2} = \frac{\partial u}{\partial Z}\frac{\partial X}{\partial Z} = \frac{\partial^2 \Phi}{\partial Z \partial X}\frac{\partial X}{\partial Z}$$

Therefore, Eq. (A-13) becomes

$$\frac{\partial \Phi}{\partial X} + \frac{Ve}{U_\infty \cos \alpha_o} \frac{\partial \Phi}{\partial Z} + K\left(1 + \frac{Ve}{U_\infty \cos \alpha_o} \frac{\partial X}{\partial Z}\right) \frac{\partial^2 \Phi}{\partial X \partial n} = 0 \qquad \text{(A-14)}$$

Furthermore, if it is assumed that the streamlines at the slotted wall are controlled principally by the cross-flow velocity (Ve), then the angle of the streamlines along the X-direction is approximately constant at the wall and equal to α_o. Therefore,

$$\frac{Ve}{U_\infty \cos \alpha_o} \frac{\partial X}{\partial Z} \approx \frac{U_\infty \sin \alpha_o}{U_\infty \cos \alpha_o} \cot \alpha_o = 1 \qquad \text{(A-15)}$$

Thus, the slotted-wall boundary condition for a wall placed normal to the direction of lift takes the form of the classic slotted/porous boundary condition derived by Baldwin, et al. (Ref. 10):

$$\frac{\partial \Phi}{\partial X} + \frac{1}{R_e} \frac{\partial \Phi}{\partial Z} + K_e \frac{\partial^2 \Phi}{\partial X \partial Z} = 0 \qquad \text{(A-16)}$$

where the pseudo porosity parameter $(1/R_e)$ is

$$\frac{1}{R_e} = \frac{Ve}{U_\infty \cos \alpha_o} = \tan \alpha_o \qquad \text{(A-17)}$$

and the effective slot parameter is

$$K_e = 2K \qquad \text{(A-18)}$$

Equation (A-16) is the slotted-wall boundary condition which can be used to determine the interference effects on V/STOL models with high cross-flow velocities.

APPENDIX B
LIST OF FUNCTIONS

The expressions for the functions A_1, A_2, B_1, and B_2 in Eq. (41) are:

$$A_1 = \frac{\left[(1 - \lambda f F)(\cosh(\lambda f) + \lambda F f \sinh(\lambda f)) - (f/qR)^2 \sinh(\lambda f)\right] e^{-\lambda f}}{\left[(\cosh(\lambda f) + \lambda F f \sinh(\lambda f))^2 + (f/qR)^2 \sinh^2(\lambda f)\right]} \tag{B-1}$$

$$A_2 = \frac{-(f/qR)}{\left[(\cosh(\lambda f) + \lambda F f \sinh(\lambda f))^2 + (f/qR)^2 \sinh^2(\lambda f)\right]} \tag{B-2}$$

$$B_1 = -\frac{\left[(1 - \lambda F f)(\sinh(\lambda f) + \lambda F f \cosh(\lambda f)) - (f/qR)^2 \cosh(\lambda f)\right] e^{-\lambda f}}{\left[(\sinh(\lambda f) + \lambda F f \cosh(\lambda f))^2 + (f/qR)^2 \cosh^2(\lambda f)\right]} \tag{B-3}$$

$$B_2 = \frac{(f/qR)}{\left[(\sinh(\lambda f) + \lambda F f \cosh(\lambda f))^2 + (f/qR)^2 \cosh^2(\lambda f)\right]} \tag{B-4}$$

The expressions c_n, d_n, D_n, E_n, F_n, G_n, M_n, N_n, P_n, and R_n in Eqs. (49) and (50) are

$$c_n = f \cos \beta_n \tag{B-5}$$

$$d_n = q \sin \beta_n \tag{B-6}$$

$$D_n = \frac{2}{\left(4a_n - b_n^2\right)}\left[\frac{2\ell_n + b_n}{r_{n_o}} - \frac{b_n}{\sqrt{a_n}}\right] \tag{B-7}$$

$$E_n = \frac{1}{r_{n_o}^3}\left[\frac{-\ell_n}{2} + \frac{b_n}{12} + \frac{(4a_n + b_n^2)}{(4a_n - b_n^2)}\,\frac{(2\ell_n + b_n)}{12}\right] + \frac{2}{3}\,\frac{(4a_n + b_n^2)}{(4a_n - b_n^2)^2}\,\frac{(2\ell_n + b_n)}{r_{n_o}} - \frac{b_n}{12a_n^{3/2}}\left[1 + \frac{4a_n + b_n^2}{4a_n - b_n^2}\right] - \frac{2}{3}\,\frac{(4a_n + b_n^2)}{(4a_n - b_n^2)^2}\,\frac{b_n}{\sqrt{a_n}} \tag{B-8}$$

$$F_n = \frac{1}{3r_{n_o}^3}\left[1 + \frac{b_n(2\ell_n + b_n)}{(4a_n - b_n^2)}\right] + \frac{8b_n(2\ell_n + b_n)}{3(4a_n - b_n^2)^2 r_{n_o}} - \frac{1}{3a_n^{3/2}}\left[1 + \frac{b_n^2}{(4a_n - b_n^2)}\right] - \frac{8b_n^2}{3(4a_n - b_n^2)^2\sqrt{a_n}} \tag{B-9}$$

$$G_n = \frac{2}{3}\frac{(2\ell'_n + b_n)}{(4a_n - b_n^2)r_{n_o}^3}\left[1 + \frac{8r_{n_o}^2}{(4a_n - b_n^2)}\right] - \frac{2}{3}\frac{b_n}{(4a_n - b_n^2)a_n^{3/2}}\left[1 + \frac{8a_n}{(4a_n - b_n^2)}\right] \quad \text{(B-10)}$$

$$M_n = d_n + c_n \sinh(c_n\ell'_n)\sin(d_n\ell'_n) - d_n \cosh(c_n\ell'_n)\cos(d_n\ell'_n) \quad \text{(B-11)}$$

$$N_n = c_n \cos(d_n\ell'_n)\sinh(c_n\ell'_n) + d_n \cosh(c_n\ell'_n)\sin(d_n\ell'_n) \quad \text{(B-12)}$$

$$P_n = d_n \sinh(c_n\ell'_n)\cos(d_n\ell'_n) - c_n \cosh(c_n\ell'_n)\sin(d_n\ell'_n) \quad \text{(B-13)}$$

$$R_n = -c_n + d_n \sinh(c_n\ell'_n)\sin(d_n\ell'_n) + c_n \cosh(c_n\ell'_n)\cos(d_n\ell'_n) \quad \text{(B-14)}$$

where

$$a_n = x_n^2 + 4k^2 + z_n^2 \quad \text{(B-15)}$$

$$b_n = -2(x_n \sin\beta_n - z_n \cos\beta_n) \quad \text{(B-16)}$$

and

$$r_{n_o} = \sqrt{a_n + b_n\ell'_n + \ell'^2_n} \quad \text{(B-17)}$$

APPENDIX C
FORTRAN IV PROGRAM FOR THE IBM 370/155

I. DESCRIPTION OF PROGRAM

A. MAIN PROGRAM

The main program receives the input data, controls the calculation of the jet trajectory and the interference factors, and prints the trajectory location and interference factors as output data.

B. EVAL

This subroutine calculates the coefficients D_n, E_n, F_n, and G_n and forms the terms of the k-series of Eq. (49) or Eq. (50).

C. FCT

This FORTRAN Function calculates A_1, A_2, B_1, B_2, c_n, d_n, M_n, N_n, P_n, and R_n and forms the integrand for the inverse Fourier integrals of Eq. (49) or Eq. (50).

D. TF

This FORTRAN Function calculates the trajectory. For the present analysis, Margason's trajectory [Eq. (51)] was used. Any trajectory equation of the form $X = X(Z, U_\infty/U_j, d_o/b, \beta_o)$ can be substituted into this function by the User.

E. BETAF

This FORTRAN Function calculates the local slope of the wake trajectory. The equation used must be compatible with the Function TF.

F. DF

This FORTRAN Function calculates the decay of the jet along the jet wake. Any user specified function of the form DF = DF(TF, BETAF) can be used.

G. LAG 32

This subroutine performs the numerical integration of the inverse Fourier transforms of Eq. (49) or Eq. (50) by a standard 32-point Laguerre integration scheme.

II. INSTRUCTIONS FOR USE

A. DEFINITION OF INPUT VARIABLES

N	Number of straight line segments approximating the curved trajectory.
XLAM	Tunnel height-to-width ratio, $\lambda = h/b$.
UE	Jet velocity ratio, U_∞/U_j
DO	Ratio of initial jet diameter to tunnel semi-height, d_o/b
BO	Initial jet angle, β_o, deg
NM	Number of x locations
XMIN	Initial x/b location
XDEL	x/b increment
P	Slot parameter
Q	Porosity parameter

B. ORDER OF DATA DECK

	Columns	Variable
Card 1	0-5	N
	6-15	XLAM
	16-25	UE
	26-35	DO
	36-45	BO
Card 2	0-5	NM
	6-15	XMIN
	16-25	XDEL

The input values for P and Q are internally generated in the main program. They are assigned the values 0.001, 0.2, 0.4, 0.6, 0.8, and 1.0. Particular values for P and Q can be generated by appropriately modifying the Data AH/card (line 7 of the main program).

C. DATA VALUES

The variables N and NM must be right justified in their fields, and punched without a decimal point. The variables XLAM, UE, DO, BO, XMIN, and XDEL must be punched with the decimal point, but need not be right justified.

D. INPUT AND OUTPUT SAMPLES

A sample input deck is shown following the program listing. The output for this case is also shown. A description of the output follows:

Line 1:	Input variables N, h/b, U_∞/U_j, d_o/b, and β_o
Line 2:	Trajectory description
Line 3:	Jet decay description
Line 4-10:	Jet trajectory geometry, β_n, ξ_n, and ζ_n for n = 0, 1, . . . , N
Line 11:	Slot and porosity parameters, P and Q, respectively
Line 12:	Values of δ_{w1}, δ_{w2}, δ_{u1}, δ_{u2}, δ_w, δ_u at the x/b locations where δ_{w1} and δ_{u1} are the contributions from the horizontal walls, δ_{w2} and δ_{u2} are the contributions from the vertical walls, and δ_w and δ_u are the total interference factors.

```
C
C      V/STOL MODEL WALL INTERFERENCE
C              USING
C      SLOTTED/POROUS BOUNDARY CONDITION
C
C
       IMPLICIT REAL*8(A-H,O-Z)
       DIMENSION ZETA(10),XI(10),A(10),B(10),C(10),DW1(10),DW2(10),
      1DU1(10),DU2(10),BETA(10),SMB(10),DFF(10)
       COMMON /PASS/ BO,DO,UE,XIN
       COMMON X(10),Z(10),XL(10),SB(10),CB(10),F,RIN,XLAM,M,I,PI,PI2
       DIMENSION AH(6)
       DATA AH/0.001D+0,0.2D+0,0.4D+0,0.6D+0,0.8D+0,1.0D+0/
       CALL ERRSET(207,256,-1,1)
       CALL ERRSET(266,256,-1,1)
       CALL ERRSET(208,256,-1,1)
  900  READ (5,500,END=999) N,XLAM,UE,DO,BO
       WRITE (6,130) N,XLAM,UE,DO,BO
       READ (5,200) NM,XMIN,XDEL
       WN=N
       PI=3.1415926265358979
       PI2=PI/2.0D+0
       XIN=TF(-XLAM,0)
       CALL DFN
       ZETAN=-XLAM
       NP1=N+1
       WRITE (6,121)
       DO 12 I=1,NP1
       ZETA(I)=ZETAN*(I-1)/WN
       XI(I)=TF(ZETA(I),0)
       DFF(I)=DF(ZETA(I),XI(I))
       BETA(I)=BETAF(ZETA(I))
       BETA(1)= BO/57.2957795131D+0
       SB(I)=DSIN(BETA(I))
       CB(I)=DCOS(BETA(I))
   12  WRITE (6,120) BETA(I),XI(I),ZETA(I)
       TEMP=ZETAN/WN
       DO 13 I=2,NP1
       T=XI(I)-XI(I-1)
       SMB(I)=DSQRT(TEMP*TEMP+T*T)
       T=DATAN(-TEMP/T)
       B(I)=PI2-BETA(I-1)-T
       C(I)=-PI2+BETA(I)+T
   13  A(I)=PI-BETA(I)+BETA(I-1)
       XL(1)=SMB(2)*DSIN(C(2))/DSIN(A(2))
       DO 14 I=2,N
   14  XL(I)=SMB(I)*DSIN(B(I))/DSIN(A(I))+SMB(I+1)*DSIN(C(I+1))/DSIN(A(I+
      11))
       XL(NP1)=SMB(NP1)*DSIN(B(NP1))/DSIN(A(NP1))
       DO 998 KR=1,6
       P=AH(KR)
       DO 998 KS=1,6
       Q=AH(KS)
       WRITE (6,156) P,Q
```

```
      F=1.0D+0/P-1.0D+0
      RIN=1.0D+0/Q-1.0D+0
      XL(NP1)=SMB(NP1)*DSIN(B(NP1))/DSIN(A(NP1))
      WRITE (6,112)
      DO 60 J=1,NM
      XX=XMIN + (J-1)*XDEL
      X(1)=XX
      Z(1)=0.0D+0
      DO 16 I=2,NP1
      IF (I.NE.2) GO TO 15
      X(I)=XL(I-1)*SB(I-1)
      Z(I)=XL(I-1)*CB(I-1)
      GO TO 16
   15 X(I)=X(I-1)+XL(I-1)*SB(I-1)
      Z(I)=Z(I-1)+XL(I-1)*CB(I-1)
   16 CONTINUE
      DO 17 I=2,NP1
   17 X(I)=XX-X(I)
      I=1
   18 DU1(I)=0.0D+0
      M=0
   19 CALL LAG32(0.0D+0,Y,1)
  190 IF (M.NE.0) Y=2.0D+0*Y
      DU1(I)=DU1(I)+Y
      IF (M.GT.250) GO TO 20
      IF (M.LT.3) GO TO 80
      IF (DABS(Y).LE.1.0D-09*DABS(DU1(I))) GO TO 20
   80 M=M+1
      GO TO 19
   20 DU1(I)=2.0D+0*XLAM*DU1(I)/PI
      IF (I.EQ.NP1) GO TO 83
      I=I+1
      GO TO 18
   83 I=1
   21 DW1(I)=0.0D+0
      M=0
   22 CALL LAG32(0.0D+0,Y,2)
      IF (M.NE.0) Y=2.0D+0*Y
      DW1(I)=DW1(I)+Y
      IF (M.GT.250) GO TO 23
      IF (M.LT.3) GO TO 81
      IF (DABS(Y).LE.1.0D-05*DABS(DW1(I))) GO TO 23
   81 M=M+1
      GO TO 22
   23 DW1(I)=2.0D+0*XLAM*DW1(I)/PI
      IF (I.EQ.NP1) GO TO 24
      I=I+1
      GO TO 21
   24 I=1
   93 DW2(I)=0.0
      K=1
   25 CALL EVAL(K,1,ANS)
      DW2(I)=DW2(I)+ANS
      IF (K.LE.3) GO TO 51
      IF (K.GT.250) GO TO 26
      IF (DABS(ANS).LE.1.0D-05*DABS(DW2(I))) GO TO 26
```

```
   51 K=K+1
      GO TO 25
   26 DW2(I)=4.0D+0*XLAM*DW2(I)/PI
      IF (I.EQ.NP1) GO TO 27
      I=I+1
      GO TO 93
   27 I=1
   94 DU2(I)=0.0D+0
      K=1
   28 CALL EVAL(K,2,ANS)
      DU2(I)=DU2(I)+ANS
      IF (K.LE.3) GO TO 50
      IF (K.GT.250) GO TO 29
      IF (DABS(ANS).LE.1.0D-05*DABS(DU2(I))) GO TO 29
   50 K=K+1
      GO TO 28
   29 DU2(I)=-12.0*DU2(I)/PI
      IF (I.EQ.NP1) GO TO 30
      I=I+1
      GO TO 94
   30 SUM1=0.0D+0
      SUM2=0.0D+0
      SUM3=0.0D+0
      SUM4=0.0D+0
      DO 40 I=1,NP1
      SUM1=SUM1+DFF(I)*DW1(I)
      SUM2=SUM2+DFF(I)*DW2(I)
      SUM3=SUM3+DFF(I)*DU1(I)
   40 SUM4=SUM4+DFF(I)*DU2(I)
      DW=SUM1+SUM2
      DU=SUM3+SUM4
      WRITE (6,120) XX,SUM1,SUM2,SUM3,SUM4,DW,DU
   60 CONTINUE
  998 CONTINUE
      GO TO 900
  999 STOP
  101 FORMAT(///,5X,'TRAJECTORY DOES NOT INTERSECT WALL',//)
  102 FORMAT(///,5X,'TRAJECTORY INTERSECTS WALL',//)
  156 FORMAT(/,5X,'P=',F5.3,5X,'Q=',F5.3,/)
  112 FORMAT(//,17X,'X',15X,'DW1',15X,'DW2',15X,'DU1',15X,'DU2',16X,
     1'DW',16X,'DU',/)
  122 FORMAT(//,24X,'A',17X,'B',17X,'C',15X,'SMB')
  121 FORMAT(21X,'BETA',16X,'XI',14X,'ZETA')
  120 FORMAT(7X,7D18.7)
  130 FORMAT (1H1,' N=',I5,3X,'LAMBDA=',F10.5,3X,'UE=',F10.5,3X,'DO=',
     1  F10.5,3X,'BO=',F10.5)
  200 FORMAT (I5,2F10.0)
 '500 FORMAT (I5,4F10.0)
      END
```

```
      SUBROUTINE EVAL(K,ICASE,ANS)
      IMPLICIT REAL*8(A-H,O-Z)
      COMMON XN(10),ZN(10),XL(10),SB(10),CB(10),F,RIN,XLAM,M,I,PI,PI2
      AN=XN(I)*XN(I)+4.0D+0*K*K+ZN(I)*ZN(I)
      SA=DSQRT(AN)
      A32=SA**3.
      BN=-2.0D+0*(XN(I)*SB(I)-ZN(I)*CB(I))
      BS=BN*BN
      V=4.0D+0*AN
      T=V-BS
      U=V+BS
      BSQA=BN/SA
      RN=AN+XL(I)*(BN+XL(I))
      SR=DSQRT(RN)
      R3=SR*SR*SR
      S=2.0D+0*XL(I)+BN
      DN=2.0D+0*(S/SR-BSQA)/T
      FN=((1.0D+0+BS/T)/A32+8.0D+0*BS/(T*T*SA)-(1.0D+0+BN*S/T)/R3  -
     1  8.0D+0*BN*S/(T*T*SR))/3.0
      FN=-FN
      GN=2.0D+0*(S*(1.0D+0+8.0*RN/T)/R3-BN*(1.0D+0+8.0D+0*AN/T)/A32) /
     1 (3.0D+0*T)
      EN=(-XL(I)+(BN+U*S/T)/6.0D+0)/(2.0D+0*R3)+2.0D+0*(U*S/SR-U*BSQA)/
     1 (3.0D+0*T*T)-BN*(1.0D+0+U/T)/(12.0*A32)
      CC=CB(I)
      IF (ICASE.EQ.2) GO TO 20
      ANS=DN-3.0D+0*ZN(I)*(ZN(I)*GN+6.0D+0*CC*FN)-3.0*EN*CC*CC
      RETURN
   20 SS=SB(I)
      ANS=ZN(I)*XN(I)*GN-(ZN(I)*SS+XN(I)*CC)*FN+CC*SS*EN
      RETURN
      END
```

```
      FUNCTION FCT(X,K)
      IMPLICIT REAL*8(A-H,O-Z)
      COMMON Y(10),Z(10),XL(10),SB(10),CB(10),F,RIN,XLAM,M,I,PI,PI2
      PM=DSQRT(X*X+M*M*PI*PI)
      PL=PM*XLAM
      EPL=DEXP(-PL)
      SPL=DSINH(PL)
      CPL=DCOSH(PL)
      PFL=F*PL
      PSI=1.D0+O-PFL
      P1=CPL+PFL*SPL
      P2=SPL+PFL*CPL
      DN=X*SB(I)
      CN=PM*CB(I)
      QX=X*Y(I)
      SQX=DSIN(QX)
      CQX=DCOS(QX)
      DL=DN*XL(I)
      CL=CN*XL(I)
      SPL2=SPL*SPL
      CPL2=CPL*CPL
      SDL=DSIN(DL)
      CDL=DCOS(DL)
      SHDL=DSINH(DL)
      CHDL=DCOSH(DL)
      SCL=DSIN(CL)
      CCL=DCOS(CL)
      SHCL=DSINH(CL)
      CHCL=DCOSH(CL)
      EMN=DN*CN*SHCL*SDL-DN*CHCL*CDL
      ENN=CN*CDL*SHCL+DN*CHCL*SDL
      PN=DN*SHCL*CDL-CN*CHCL*SDL
      RN=-CN+DN*SHCL*SDL+CN*CHCL*CDL
      ZPM=PM*Z(I)
      CHZPM=DCOSH(ZPM)
      SHZPM=DSINH(ZPM)
      CNDN=CN*CN+DN*DN
      S=PM*RIN/X
      S2=S*S
      DENOM= P1*P1+S2*SPL2
      A11= (PSI*P1-S*SPL)*EPL / DENOM
      A12= -S / DENOM
      DENOM=P2*P2+S2*CPL2
      B11=(-PSI*P2+S2*CPL)*EPL / DENOM
      B12= S/ DENOM
      IF (K.EQ.2) GO TO 20
      T1=A11*CHZPM*(PN*CQX+RN*SQX)
      T2=A12*CHZPM*(PN*SQX-RN*CQX)
      T3=B11*SHZPM*(EMN*CQX-ENN*SQX)
      T4=B12*SHZPM*(ENN*CQX+EMN*SQX)
      FCT= (T1+T2+T3+T4)*X/CNDN
      RETURN
   20 T1=A11*SHZPM*(PN*SQX-RN*CQX)
      T2=-A12*SHZPM*(PN*CQX+RN*SQX)
      T3=B11*CHZPM*(ENN*CQX+EMN*SQX)
      T4=B12*CHZPM*(ENN*SQX-EMN*CQX)
      FCT= (T1+T2+T3+T4)*PM/CNDN
      RETURN
      END
```

```
      FUNCTION TF(X,K)
      IMPLICIT REAL*8(A-H,O-Z)
      COMMON /PASS/ BO,DO,UE,XIN
      DATA II/0/
      IF (II.EQ.0) WRITE (6,100)
      II=1
  100 FORMAT (///,5X,'MARGASON''S TRAJECTORY')
      TF=-0.25D+0*UE*UE*X**3/(DO*DO*DCOSD(BO)**2) - X*DSIND(BO)/DCOSD(BO
     1)
      IF (K.EQ.0) RETURN
      TF=TF-XIN
      RETURN
      END



      FUNCTION BETAF(X)
      IMPLICIT REAL*8(A-H,O-Z)
      COMMON /PASS/ BO,DO,UE
      A=0.75D+0*UE*UE*X*X/(DO*DO*DCOSD(BO)**2) + DSIND(BO)/DCOSD(BO)
      BETAF= DATAN(A)
      RETURN
      END



      FUNCTION UF(X,Y)
      IMPLICIT REAL*8(A-H,O-Z)
      COMMON /PASS/ BO,DO,UE
      UF=1.0D+0
      RETURN
      ENTRY OPN
      WRITE (6,100)
  100 FORMAT(///,5X,'CONSTANT STRENGTH JET')
      RETURN
      END
```

```
      SUBROUTINE LAG32(A,Y,K)
      DOUBLE PRECISION X,Y,A
      FCT1(X)=DEXP(X)*FCT(X+A,K)
      X=.1117513980979380 03
      Y=.4510536193898970-47*FCT1(X)
      X=.9882954286828400 02
      Y=Y+.1338616942106260-41*FCT1(X)
      X=.8873534041789240 02
      Y=Y+.2671511219240140-37*FCT1(X)
      X=.8018744697791350 02
      Y=Y+.1192248760098220-33*FCT1(X)
      X=.7268762809066270 02
      Y=Y+.1913375494454220-30*FCT1(X)
      X=.6597537728793510 02
      Y=Y+.1418560545463040-27*FCT1(X)
      X=.5989250916213400 02
      Y=Y+.5661294130397360-25*FCT1(X)
      X=.5433372133339690 02
      Y=Y+.1346982586637400-22*FCT1(X)
      X=.4922439498730860 02
      Y=Y+.2054429673788050-20*FCT1(X)
      X=.4450920799575490 02
      Y=Y+.2119792290163620-18*FCT1(X)
      X=.4014571977153940 02
      Y=Y+.1542133833393820-16*FCT1(X)
      X=.3610049480575200 02
      Y=Y+.8171823443420720-15*FCT1(X)
      X=.3234662915396470 02
      Y=Y+.3237801657729270-13*FCT1(X)
      X=.2886210181632350 02
      Y=Y+.9799379288727090-12*FCT1(X)
      X=.2562863602245920 02
      Y=Y+.2305899491891340-10*FCT1(X)
      X=.2263088901319680 02
      Y=Y+.4281382971040930-09*FCT1(X)
      X=.1985586094033610 02
      Y=Y+.6350602226625810-08*FCT1(X)
      X=.1729245433671530 02
      Y=Y+.7604567879120780-07*FCT1(X)
      X=.1493113975552260 02
      Y=Y+.7416404578667550-06*FCT1(X)
      X=.1276369798674270 02
      Y=Y+.5934541612868630-05*FCT1(X)
      X=.1078301863254000 02
      Y=Y+.3920341967987950-04*FCT1(X)
      X=.8982940924212600 01
      Y=Y+.2148649188013640-03*FCT1(X)
      X=.7358126733186240 01
      Y=Y+.9808033066149550-03*FCT1(X)
      X=.5903958504174240 01
      Y=Y+.3738816294611520-02*FCT1(X)
      X=.4616456769749770 01
      Y=Y+.1191821483483860-01*FCT1(X)
      X=.3492213273021990 01
```

```
      Y=Y+.3176091250917510-01*FCT1(X)
      X=.2528336706425790 01
      Y=Y+.7057862386571740-01*FCT1(X)
      X=.1722408776444650 01
      Y=Y+.1299837862860720 00*FCT1(X)
      X=.1072448753817820 01
      Y=Y+.1959033359728810 00*FCT1(X)
      X=.5768846293018860 00
      Y=Y+.2352132296698480 00*FCT1(X)
      X=.2345261095196190 00
      Y=Y+.2104431079388130 00*FCT1(X)
      X=.4448936583326700-01
      Y=Y+.1092183419523850 00*FCT1(X)
      RETURN
      END
```

TYPICAL INPUT DATA

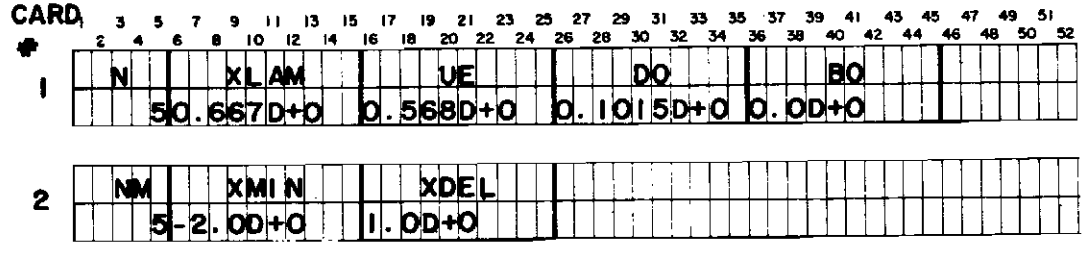

TYPICAL OUTPUT DATA

N= 5 LAMBDA= 0.66700 UE= 0.56800 DO= 0.10150 BO= 0.0

MARGASON'S TRAJECTORY

CONSTANT STRENGTH JET

BETA	XI	ZETA
0.0	0.0	0.0
0.3958949D 00	0.1858541D-01	-0.1334000D 00
0.1031746D 01	0.1486833D 00	-0.2668000D 00
0.1310966D 01	0.5018060D 00	-0.4002000D 00
0.1422361D 01	0.1189466D 01	-0.5336000D 00
0.1475385D 01	0.2323176D 01	-0.6670000D 00

P=0.200 Q=0.400

X	DW1	DW2	DU1	DU2	DW	DU
-0.2000000D 01	-0.6557777D-01	0.8279613D-01	-0.3562120D-01	0.2051757D-01	0.1721836D-01	-0.1510363D-01
-0.1000000D 01	-0.1804475D 00	0.1406769D 00	-0.1534477D-01	0.3323180D-01	-0.3977061D-01	0.1788703D-01
0.0	0.2110010D 00	0.2204982D 00	0.2415443D 00	0.2175276D-01	0.4314992D 00	0.2632970D 00
0.1000000D 01	0.9022103D 00	0.2563343D 00	0.2508667D 00	-0.5117537D-01	0.1158545D 01	0.1996913D 00
0.2000000D 01	0.1270115D 01	0.2148716D 00	-0.2180011D 00	-0.1138828D 00	0.1484987D 01	-0.3318838D 00

NOMENCLATURE

A	Area of jet
A_1, A_2	Series coefficients, Appendix B
a	Width of a slot
B_1, B_2	Series coefficients, Appendix B
b	Semiwidth of rectangular wind tunnel
C	Cross-sectional area of rectangular tunnel, 4hb
c_n	f cos β_n
D_n	Series coefficient, Appendix B
d	Slot spacing
d_n	q sin β_n
d_o	Initial jet diameter
E_n	Series coefficient, Appendix B
F	Normalized geometric slot parameter, K/h
F_n	Series coefficient, Appendix B
f	$(q^2 + m^2\pi^2)^{1/2}$
G_n	Series coefficient, Appendix B
h	Semiheight of rectangular wind tunnel
J. I. P	Jet intersection point with tunnel boundary
K	Geometric slot parameter, Eq. (4)
K_e	Equivalent slot parameter for quasi-linear boundary condition, 2K
L_n	Length of nth straight line segment approximation to curved wake
ℓ_n	Normalized segment length, L_n/b
M_n	Series coefficient, Appendix B
m	y-coordinate Fourier transform parameter
N	Number of straight line segments approximating the curved wake

N_n	Series coefficient, Appendix B
P	Slot parameter, $(1 + F)^{-1}$; P = 0 is closed wall and P = 1 is open jet
P_n	Series coefficient, Appendix B
p	Local static pressure
p_∞	Free-stream static pressure
p_{t_∞}	Free-stream total pressure
Q	Porosity parameter, $(1 + 1/R)^{-1}$, Q = 0 is closed wall and Q = 1 is open jet
q	x-coordinate Fourier transform parameter
R	Porosity parameter
R_e	Pseudo porosity parameter for quasi-linear boundary condition, Eq. (7)
R_n	Series coefficient, Appendix B
r	Distance from any field point to element of vortex ring representing the V/STOL model
S	Distance along the jet
s	Normalized distance along the jet, S/b
U_j	Initial jet velocity
U_∞	Free-stream velocity
u_h	Perturbation velocity in axial direction induced by horizontal walls
u_i	Interference perturbation velocity in axial direction, $\partial\phi_i/\phi_x$
w_i	Interference perturbation velocity in vertical direction, positive downward, $\partial\phi_i/\partial z$
w_o	Average velocity at rotor disk, $1/2\ (d\gamma/ds)$
X, Y, Z	Cartesian coordinates in physical dimensions
x, y, z	Normalized cartesian coordinates, X/b, Y/b, Z/b
α_o	Zero-lift angle of attack
β	Inclination angle between wake trajectory and vertical axis

β_o	Initial wake angle
Γ	Circulation
γ	Normalized circulation, $\Gamma / U_\infty b$
δ_u	Streamwise interference factor, $(Cu_i)/(Aw_o)$
δ_w	Upwash interference factor, $(Cw_i)/(Aw_o)$
ζ	Z location of jet doublet
θ	Vortex angle
λ	Tunnel height-to-width ratio, h/b
ξ	X location of jet doublet
Φ	Perturbation velocity potential
ϕ	Normalized perturbation velocity potential, $\Phi / U_\infty b$
ϕ_h	Normalized perturbation velocity potential due to the horizontal walls
ϕ_i	Normalized interference velocity potential
ϕ_m	Normalized perturbation velocity potential due to the model
ϕ_v	Normalized velocity potential for an infinite row of model images